Geomorphology 277 (2017) 100–117

Contents lists available at ScienceDirect

Geomorphology

journal homepage: www.elsevier.com/locate/geomorph

Toward a conceptual model relating chemical reaction fronts to water flow paths in hills

Susan L. Brantley [a,b,*], Marina I. Lebedeva [a], Victor N. Balashov [a], Kamini Singha [c], Pamela L. Sullivan [d], Gary Stinchcomb [e]

[a] Earth and Environmental Systems Institute, Pennsylvania State University, University Park, PA 16802, USA
[b] Department of Geosciences, Pennsylvania State University, University Park, PA 16802, USA
[c] Department of Geology and Geological Engineering and Hydrologic Science and Engineering Program, Colorado School of Mines, Golden, CO 80401, USA
[d] Department of Geography and Atmospheric Sciences, University of Kansas, Lawrence, KS 66045, USA
[e] Department of Geosciences and Watershed Studies Institute, Murray State University, Murray, KY 40271, USA

ARTICLE INFO

Article history:
Received 25 October 2015
Received in revised form 5 September 2016
Accepted 12 September 2016
Available online 14 September 2016

Keywords:
Hillslope hydrology
Weathering
Geochemistry
Erosion

ABSTRACT

Both vertical and lateral flows of rock and water occur within eroding hills. Specifically, when considered over geological timeframes, rock advects vertically upward under hilltops in landscapes experiencing uplift and erosion. Once rock particles reach the land surface, they move laterally and down the hillslope because of erosion. At much shorter timescales, meteoric water moves vertically downward until it reaches the regional water table and then moves laterally as groundwater flow. Water can also flow laterally in the shallow subsurface as interflow in zones of permeability contrast. Interflow can be perched or can occur during periods of a high regional water table. The depths of these deep and shallow water tables in hills fluctuate over time. The fluctuations drive biogeochemical reactions between water, CO_2, O_2, and minerals and these in turn drive fracturing. The depth intervals of water table fluctuation for interflow and groundwater flow are thus reaction fronts characterized by changes in composition, fracture density, porosity, and permeability. The shallow and deep reaction zones can separate over meters in felsic rocks. The zones act like valves that reorient downward unsaturated water flow into lateral saturated flow. The valves also reorient the upward advection of rock into lateral flow through solubilization. In particular, groundwater removes highly soluble, and interflow removes moderately soluble minerals. As rock and water moves through the system, hills may evolve toward a condition where the weathering advance rate, W, approaches the erosion rate, E. If $W = E$, the slopes of the deep and shallow reaction zones and the hillsides must allow removal of the most soluble, moderately soluble, and least soluble minerals respectively. A permeability architecture thus emerges to partition each evolving hill into dissolved and particulate material fluxes as it approaches steady state.

1. Introduction

The largest supply of accessible, potable water is contained in rocks beneath our feet (Fetter, 2001). To learn to sustain our water supply, we need conceptual and numerical models that describe how water is stored and how it moves through rock and regolith. At present, we cannot predict such hydrologic partitioning because of the extremely heterogeneous distribution of subsurface rock material (Gleeson et al., 2015).

A major thrust of critical zone science is to develop models of weathering and landscape evolution to allow a priori predictions of the architecture of mineralogy, porosity, and permeability in regolith (e.g., Carson and Kirkby, 1972; Anderson et al., 2002; Amundson, 2004; Mudd and Furbish, 2004; Godderis et al., 2006; Lebedeva et al., 2007; Minasny et al., 2008; Pelletier, 2008; Yoo and Mudd, 2008; Burke et al., 2009; Lebedeva et al., 2010; Brantley and Lebedeva, 2011; Rasmussen et al., 2011; Lebedeva and Brantley, 2013; Duffy et al., 2014; Rempe and Dietrich, 2014). Here, we use the term regolith to mean all the fragmented and altered material that overlies pristine bedrock (protolith). Major advances have also been made in the last two decades in relating hillslope hydrology to the compartmentalization of water chemistry inside hills (e.g., Hooper et al., 1990; McDonnell, 1990; Tromp-van Meerveld and McDonnell, 2006; Legout et al., 2007; Ayraud et al., 2008; Katsura et al., 2008; Salve et al., 2012; van Meerveld et al., 2015). However, these two sets of approaches have largely been separate, and we generally cannot relate the flux of solutes out of a catchment to where weathering is occurring at depth (e.g., Calmels et al., 2007; Legout et al., 2007). This lack of detailed understanding of weathering inside individual hills may have implications at global scales (Torres et al., 2014).

---

* Corresponding author at: Earth and Environmental Systems Institute, Pennsylvania State University, University Park, PA 16802, USA.
E-mail address: brantley@geosc.psu.edu (S.L. Brantley).

http://dx.doi.org/10.1016/j.geomorph.2016.09.027
0169-555X/© 2016 Published by Elsevier B.V.

Given this state of the science, when catchments are studied, the hydrologist does not know which of several conceptual models to apply (Welch and Allen, 2014). For upland systems, for example, researchers have used (i) a bucket-type model where the subsurface is not layered, (ii) a one-layer approach where subsurface flow is restricted to an upper layer and bedrock is considered impermeable, or (iii) a two-flow approach where lateral flow occurs in an upper layer and in a lower layer (Banks et al., 2009).

Here, we explore the idea that the compartments and layers described by hydrologists (Dewandel et al., 2006; Ayraud et al., 2008) and water masses described by river investigators (Calmels et al., 2007) may be related to reaction fronts mapped at depth by geochemists (Brantley et al., 2013a). These reaction fronts are depth intervals in the subsurface where reactions are occurring. Beneath hills in humid systems where net unsaturated water flow is vertical, for example, minerals can dissolve or precipitate to form reaction fronts that roughly mimic the land surface (Figs. 1, 2). In the presence of very impermeable rock, solutes are transported across reaction fronts by diffusion; in contrast, in high-flow, permeable rock, solute transport is dominated by advection. In this paper we explore the idea that reaction fronts for different minerals separate over space (Figs. 2B,C) when solutes move through the fronts largely by advection. In contrast, the fronts remain co-located within tens of centimeters (Fig. 2A) when solute transport is largely by diffusion. We try to relate these fronts to hillslope hydrology by developing a conceptual model.

Specifically, the mineral assemblages observed across reaction fronts can reveal information about the cumulative water flows. These mineral assemblages can magnify relative differences in fluid flow in different layers because the solubility of minerals is small when considered on a volume/volume basis (volume of dissolved mineral / volume of water). Such dimensionless solubilities generally are ~10^{-3} or smaller (Berner, 1981). This means that the volume of water that must flow through a given rock matrix to dissolve and remove a mineral is $>10^3$ times the volume of mineral that is dissolving. Small differences in reacted mineral volumes across depth intervals thus can record and magnify differences in cumulative water flow.

We exemplify these ideas with field data for shale, granite, and diabase (Fig. 2). We emphasize one physiographic province, the Piedmont of the eastern U.S.A., where long exposure times and low erosion rates are likely to have resulted in geomorphological steady state (Pavich, 1986; Pavich et al., 1989). We also discuss an example from the Susquehanna Shale Hills Critical Zone Observatory situated just to the north of Virginia where isotope-based estimates of the erosion rate and the soil production rate at ridgetops are equal within error (West et al., 2013).

The point of the paper is to use a critical zone science approach, i.e., an approach that explores how geochemical, hydrological, and geomorphological observations can illuminate the question of water flow inside hills. Although the treatment is qualitative in comparison to state-of-the-art geochemical, hydrological, or geomorphological studies, the concepts are explored to stimulate the development of better conceptual models for hills.

In the models presented here, we first consider hills where mean annual precipitation (MAP) exceeds potential evapotranspiration (ET), and where regolith formation conceptualized in one or two dimensions (1D or 2D) consists of net water flow downward occurring at relatively fast timescales and net rock material flow upward at geologic timescales. Vegetation also takes up material but this represents a short-term cycle (<100 years) in which material is stored and returned to the system; this biotic cycle is thus largely ignored. Throughout the paper we emphasize models where rates of uplift (U), weathering (W), erosion (E), and channel incision (I) are all equal. We call these *steady state* models because aspects of the regolith and its distribution do not vary with time; others refer to models where $E = U$ as *dynamic equilibrium* (Hack, 1960; Pain and Ollier, 1996). We extend such ideas by including implications of weathering advance rates in this steady state model.

2. A geochemical model of hillslope evolution

Since the 1980s, 1D numerical reactive transport models have described weathering caused by interaction of meteoric water with minerals (e.g., Lichtner, 1988; Lichtner and Waber, 1992; Steefel, 1993). More recently, reactive transport models have been used to describe regional-scale weathering under landscapes (e.g., Maher, 2011). Reactive-transport models have also been extended to include physical erosion (Waldbauer and Chamberlain, 2005; Lebedeva et al., 2007; Hilley et al., 2010; Lebedeva et al., 2010; Brantley and Lebedeva, 2011; Brantley et al., 2013b). Here we emphasize published models from Lebedeva and Brantley and coworkers (Lebedeva et al., 2007; Lebedeva et al., 2010; Lebedeva and Brantley, 2013) and we refer to those models throughout as L&B. In these weathering + erosion models, the rate of change of regolith thickness is simulated as the balance between the rate that weathering advances into the rock (W, in units of $\mathrm{L\,T^{-1}}$) and the rate of erosion, E ($\mathrm{L\,T^{-1}}$). When $W = E$, the regolith thickness H is constant in time (i.e., steady state). Although such a steady state has generally not been proven for individual sites, the presence of moderately thick regolith in many locations documents that neither $W >> E$ nor that $E >> W$ for geologically long periods of time. This in turn suggests that feedback mechanisms may couple erosion at the land surface to weathering and vice versa in some locations (e.g., Carson and Kirkby, 1972; Stallard, 1995; Fletcher et al., 2006; Lebedeva et al., 2007; Fletcher and Brantley, 2010; Behrens et al., 2015). Thus, regolith-mantled systems may not constantly maintain $W = E$, but they may commonly be moving toward such a steady state, driven by feedbacks. Feedbacks could include the effects of porewater chemistry, soil gas chemistry, particle size or fracture spacing (Fletcher et al., 2006; Fletcher and Brantley, 2010; Behrens et al., 2015).

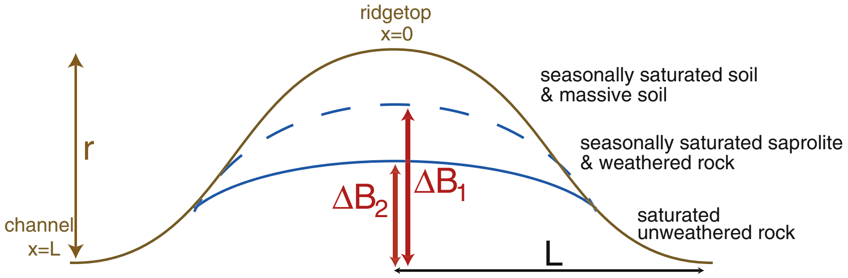

Fig. 1. Schematic hillslope showing L (distance from the divide to the channel head along the x axis), ΔB_2 (relative elevation of unweathered rock above the elevation of the channel head), ΔB_1 (relative elevation of the base of interflow above the elevation of the channel head), and r (elevation of ridgetop above the channel head). The groundwater flux Q_{gw} ($\mathrm{L^3\,T^{-1}}$) is localized at the solid line, and the interflow water flux Q_{int} ($\mathrm{L^3\,T^{-1}}$) is localized at the dashed line. Although not shown, H is the total thickness of regolith and is equivalent to $r - \Delta B_2$ under the hilltop (located at $x = 0$). In other words, regolith is here defined to include all weathered or altered material.

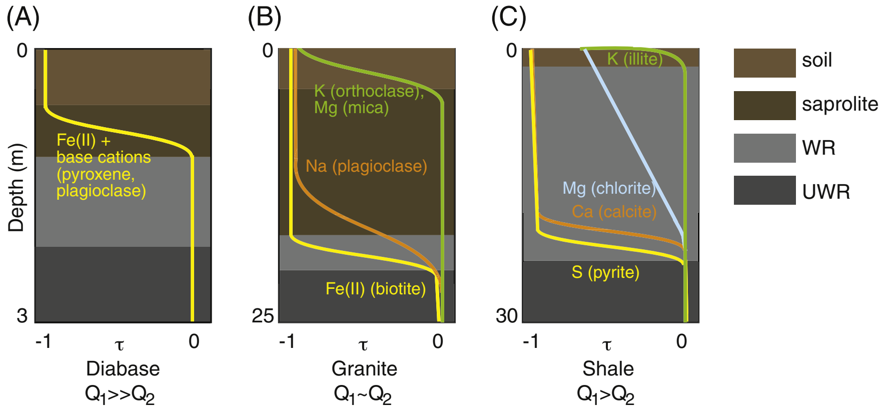

Fig. 2. Schematics showing reaction fronts within regolith at ridgetops for three systems. The upper surface is the land surface (see text). Here τ is the fractional depletion of each mineral or component compared to immobile element in the protolith. A depletion of 0% is plotted as 0 and 100% depletion is plotted as -1. (A) Diabase in the Virginia Piedmont, where reaction fronts largely do not separate. The profile-initiating mineral is high-Fe(II) pyroxene, the major-porosity initiating mineral is augite, and the soil-initiating mineral is plagioclase. (B) Granite in the Virginia Piedmont, where reaction fronts separate over tens of meters. The profile-initiating reaction is biotite oxidation, the major porosity-initiating reaction is plagioclase dissolution, and the soil-initiating reaction is dissolution of alkali-containing minerals (orthoclase feldspar, mica). (C) Rose Hill shale from central Pennsylvania, where reaction fronts separate over tens of meters. The profile-initiating mineral reaction is shown as pyrite oxidation, the major porosity-initiating reaction as carbonate dissolution, and the soil-initiating reaction as illite dissolution. (It has not been possible to distinguish whether the deepest reaction involves pyrite or carbonate, but pyrite oxidation is shown here to be deepest, for simplicity. Likewise the carbonate mineral varies from ankerite to calcite but is shown here as calcite for simplicity.) Data from Bazilevskaya et al. (2013, 2014); Jin et al. (2010), Pavich et al. (1989).

To explore controls on weathering and eroding systems, L&B formulated models that contain only a few minerals. In several models, they considered rock composed of one inert (quartz) and one reactive mineral (albite feldspar). Albite reacts to form a soil mineral (kaolinite) plus an aqueous solute component ($NaSi_2$). Some L&B models also include a redox-active mineral component (FeO). These four-mineral models focus on the two most essential chemical weathering reactions: acid consumption (albite to kaolinite) and oxidation (ferrous iron to ferric iron minerals). Quartz is included to maintain isovolumetric weathering.

Weathering reactions occur in the model as soluble reactants are transported to mineral surfaces, and products are transported away from the surfaces by advection or diffusion or both. In L&B models with advection, the advective velocity is held constant even though porosity and mineral surface area change during reaction (Lebedeva et al., 2007).

For example, L&B explored the distribution of regolith on a convex-upward hillslope (Lebedeva and Brantley, 2013). Water flows downward at a constant velocity. Solute is transported by this vertical advection as well as by vertical and horizontal diffusion. Fig. 3 shows numerical simulations from such a reactive-transport problem formulated for a quartz + albite protolith bounded by a hillslope surface that can vary over space and time. Here y and x are measured in the vertical and horizontal directions respectively, and t is time. The hillslope evolves based on the following 2D equation:

$$\frac{\partial(\phi C)}{\partial t}=\frac{\partial}{\partial x}\left(D\phi\frac{\partial C}{\partial x}\right)+\frac{\partial}{\partial y}\left(D\phi\frac{\partial C}{\partial y}\right)-\frac{\partial(Cq_x)}{\partial x}-\frac{\partial\left(Cq_y\right)}{\partial y}+j(C,\eta) \tag{1}$$

where D (m^2/s) is the diffusion coefficient in the aqueous pore solution reduced by tortuosity, and $q_x$and q_y(m/s) are the horizontal and vertical (directed downward) components of the Darcy velocity of the pore fluid, respectively. Both components are included in the equation for completeness, although q_x is set to zero in the model. The concentration of the solute released to the pore fluid is C and the albite reaction rate is j (mol/m^3 s). The extent of reaction, η (unitless), is defined as $\eta=(\rho^0-\rho)/\rho^0$. It changes with time as follows:

$$\frac{\partial\eta}{\partial t}=\frac{j(C,\eta)}{\rho^0} \tag{2}$$

Here, $\rho=\phi_{ab}/V_{ab}^0$ is the concentration of reacting mineral (albite) in the rock (superscript 0 refers to protolith composition), ϕ_{ab} is the volume fraction of albite in a rock, and V_{ab}^0 is its specific volume. The concentration of the solute in pore fluid at the land-atmosphere surface is maintained constant and equal to C^R.

Mass balance on the hillslope is written in terms of hillslope elevation Y as:

$$\rho_s\frac{\partial Y}{\partial t}=\kappa\rho_s\frac{\partial^2 Y}{\partial x^2}+(\rho_s-\rho_r)\frac{\partial\Delta B_2}{\partial t}-F(C,\eta) \tag{3}$$

Here, ρ_r and ρ_s are the bulk density of the rock and the kaolinite-containing soil, respectively; κ(m^2 y^{-1}) is the soil diffusivity (i.e., Gilbert's constant) that is used in the diffusion-like transport law describing soil flux along a hillslope (Carson and Kirkby, 1972). The position of the bedrock surface, $\Delta B_2(x,t)$ is defined as the point where protolith has experienced 0% alteration (Fig. 1). The function F describes the rate of change in material mass because of chemical processes. Assuming (i) that the solute flux is a small contributor to elevation change compared to the physical erosion flux or (ii) that weathering is isovolumetric, F can be neglected in this equation. The weathering advance rate, W, defines the elevation of unweathered material ΔB_2:

$$\frac{\partial\Delta B_2}{\partial t}=-W \tag{4}$$

At steady state, the regolith thickness, $H=r-\Delta B_2$, is constant (Fig. 1). Under this condition and neglecting the term F (Carson and Kirkby, 1972; Follain et al., 2006), Lebedeva and Brantley (2013) separated the systems of Eqs. (1)–(2) and (3)–(4) and derived the equation for the steady state (parabolic) hillslope:

$$Y_s(x)=-\frac{\rho_r E}{2\rho_s\kappa}x^2+Y_L+\frac{\rho_r E L^2}{2\rho_s\kappa} \tag{5}$$

Here, Y_L is the elevation at the channel bottom at $x=L$. As defined above, E (LT^{-2}) is the velocity of lowering of the hill because of physical erosion. The boundary condition at the channel ($x=L$) is defined so that E = the incision rate I (i.e., $Y=H_L-It$). Lebedeva and Brantley (2013) explore the idea that weathering advance is controlled by solubility and geochemical kinetics coupled with transport in a pore fluid. Note that in contrast to the multiple reaction fronts shown in Fig. 2

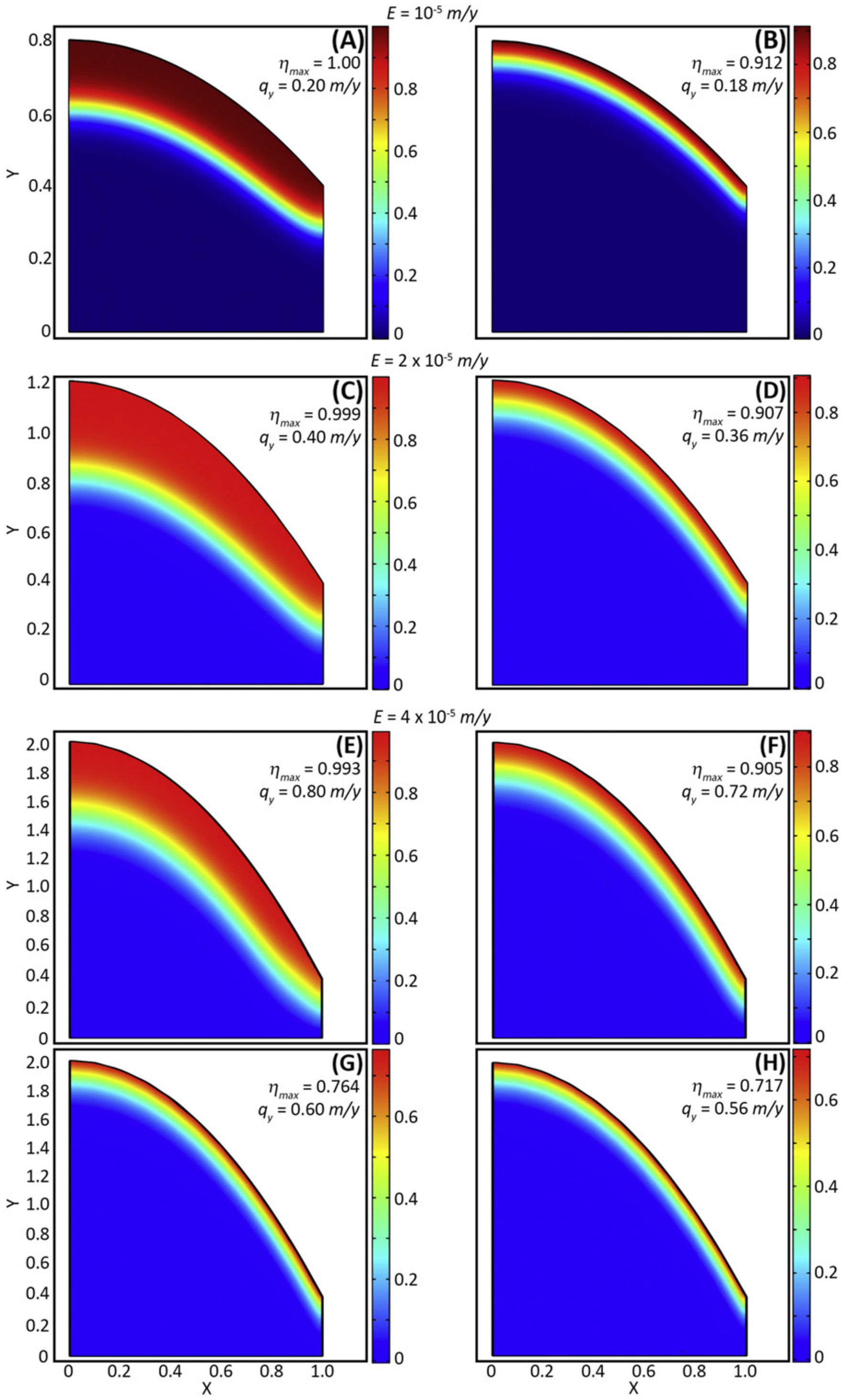

Fig. 3. (A)–(H) Simulated steady-state hillslopes calculated for the model in Eqs. (1)–(5) for different values of erosion rate *E* and vertical Darcy velocity q_y for rock of composition 40% albite and 50% quartz. The model simulate albite weathering to kaolinite (quartz is inert). Colors show contours for the extent of reaction (i.e., the extent of weathering at each depth). Unweathered bedrock is represented by blue: warmer colors represent greater extent of reaction and thus greater fraction of kaolinite (see key to right of each diagram). When 100% of the albite is reacted to kaolinite (+pore space), extent of reaction = 1. For the simulations, L = 20 m and axes are presented as dimensionless numbers normalized by this length. Other parameters in Eq. (5) were held constant. See further information in caption of Fig. 5.

and discussed later in this paper, the L&B model was formulated for the simplified rock, quartz + albite transforming to quartz + kaolinite, so only one reaction front occurs in the system. The elevation of this single front is referred to here as ΔB_2.

3. Simulated hillslopes from the L&B model

Simulated steady state hillslopes calculated using Eq. (5) and Eqs. (1)–(2) at the lowering hillslope surface are shown for various values of erosion E and vertical Darcy velocity q_y in Fig. 3. All other parameters (κ, ρ_r, ρ_s, Y_L, L, D) were held constant, and water was only allowed to flow vertically. The hillform varies only with E because the topography is affected by erosion but not by chemical weathering as described for Eq. (5). In contrast, the extent of alteration of the hill varies not only with E but also with q_y. This is because E sets the residence time in the weathering zone and q_y sets the volume of water that interacts with the mineral while it is in that zone.

All model predictions were calculated with reasonable kinetic constants for a rock with 40% albite, 50% quartz, and 10% porosity (Lebedeva et al., 2007). Fig. 3 leads to two important observations. First, the hillslope becomes steeper as E increases (Figs. 3A-3E). In fact, at steady state, the ratio of relief, r, divided by length, L, of the hill derived from mass balance on the hill (Eq. 5) yields:

$$\frac{r}{L} = \frac{EL}{\kappa}\frac{\rho_r}{2\rho_s} \approx \frac{EL}{\kappa} \tag{6}$$

The ratio r/L is roughly the slope of the convex-upward hill surface. The value of the slope of the hill can be considered an emergent property of the eroding system.

The second observation is that a thicker regolith develops at valley and at ridgetop when infiltration, q_y, increases but E is maintained constant (Fig. 3E,F vs. 3G,H). Above a critical value of q_y, however, the rate of erosion is slower than weathering advance (Lebedeva et al., 2010), and regolith thickens with time without reaching steady state (not shown). At the other extreme where I $(=E)$ increases to high values, advection velocity becomes less significant in affecting regolith thickness. Eventually, for a given lithology exposed to a given climate, a critical erosion rate is reached above which the weathering rate can no longer keep up with the erosion rate. At this point, bedrock emerges at the land surface (not shown). Like the slope of the hill, the regolith thickness is an emergent property of the system.

Another emergent property that characterizes a system and is easily observed is the extent of weathering of material emerging at the land surface, η_{max}. For an easily erodible rock that contains only moderately soluble minerals (Figs. 3B,D,F–H), mineral grains pass through the weathering zone without dissolving away entirely by the time they reach the land surface: this results in 'incompletely developed profiles' because depletion of the mineral does not equal 100% at the land surface (Brantley and White, 2009). For this case, $\eta_{max} < 1$ and such a regime has been termed 'weathering-limited' (Lebedeva and Brantley, 2013) or 'reaction-limited' (Hilley et al., 2010). An example where the dominant reactive mineral in protolith (illite) comprises an incompletely developed profile at both the ridge and valley is observed in the Susquehanna Shale Hills Critical Zone Observatory in Pennsylvania in the USA (Jin et al., 2010). At that site the dominant lithology is shale—a rock that is easily eroded but which contains relatively insoluble minerals. This site is discussed further in Section 5.

The opposite case of a lithology with a high capacity to be weathered but a lower capacity to be eroded will evolve to a 'completely developed profile'. In this type profile, the reactive mineral approaches 100% depletion at the land surface at ridge and at valley (Figs. 3A,C,E): in other words, the time needed for the mineral grains to move from the underlying protolith interface upward to the land surface is long enough that the mineral dissolves away completely and concentration drops to 0% at the land surface. This regime has been termed 'erosive transport-limited' by L&B because neither the extent of reaction at the regolith-air surface (η_{max}) nor the hill-integrated alteration rate is a function of the dissolution rate constant. The idea of a regime that is limited by the rate of physical removal of material from the weathering zone was introduced long ago (e.g., Stallard and Edmond, 1983) and has been labelled with several names. In this regime, $\eta_{max} = 1$ and can only be lowered from 1 by increasing E.

An intermediate mixed-control regime can occur such that the profile for the reacting mineral is completely developed at the ridgetop ($\eta_{max} = 1$) but is incompletely developed at the valley ($\eta_{max} < 1$). In this case the overall hill-integrated alteration rate is affected by changes in weathering rate constants and in erosional efficiency, i.e., the mixed-control or transition regime of L&B. Fig. 3H approaches this case. Examples of this are observed on metapelites, granites, and diabase in the Piedmont of Maryland and Virginia in the USA. (Cleaves et al., 1970; Pavich et al., 1989) where bedrock is exposed in the channel ($\eta_{max} = 0$) but reactions go to completion under the ridgetop ($\eta_{max} = 1$). Such cases are discussed in Section 5.

The fraction of mass solubilized from these hills varies under these different regimes. In the literature, this fraction has been referred to as the chemical depletion fraction or CDF (Riebe et al., 2001). The CDF has been calculated to describe samples, pedons, hillslopes, and watersheds. For any given sample, CDF is identical to the weathering intensity η (Brantley and Lebedeva, 2011), and can thus vary from 0 to 1. For our model hills, the CDF is the mass fraction of the hill lost as solute (see supplemental information). Our steady state models show that if E is increased but q_y is maintained constant, CDF decreases because the residence time of rock material in the weathering zone decreases. For a 1D model with constant q_y, for example, CDF varies approximately as $1/E$ in the weathering-limited regime (CDF < 1 in Fig. 4A).

If q_y increases while E is held constant in our steady state hills, the value of W $(\mathrm{L\,T^{-1}})$ still remains constant. This is because at steady state, $E = W$ $(\mathrm{L\,T^{-1}})$ = a constant. Thus, as q_y increases at constant E, the value of CDF integrated over the entire hill must increase to increase the weathering solute flux out of the hill while maintaining the same W (Fig. 4A). For example, Fig. 4B shows that CDF increases almost linearly with q_y at constant E in the weathering limited or mixed-control regimes until the regime of erosive transport limitation where CDF = 1. It may seem confusing that the weathering advance rate W can remain constant at the same time that the fraction of hill volume that leaves the hill as solute (CDF) increases. In effect, in these steady state hills, W is constrained to always equal E, and E determines the residence time that particles remain in the weathering zone. The extent of reaction is dictated by the volume of water that interacts with the mineral in the zone, i.e., it depends on q_y. For higher q_y, more weathering occurs during the transit of particles through the zone and results in a higher extent of reaction at the regolith-air surface (η_{max}), even though W remains constant.

In effect, the CDF is another emergent property of the steady state system. For this model, the CDF is determined by (i) q_y, (ii) lithology, and (iii) imposed uplift or erosion rate (where $U = E = W$). For the model hill, advection, lithology, and uplift rate set three important conditions with respect to the reactive mineral: respectively, (i) the volume of water interacting with the mineral, (ii) the initial volumes of minerals, and (iii) the duration of interaction with weathering fluids. Thus, the hill is determined by (i) climate, (ii) reactive mineral content, and (iii) tectonics. Although we emphasize the climate variable q_y rather than temperature, temperature is implicitly important because temperature affects the reaction kinetics and solubilities.

In addition to CDF, the porosity is also an emergent property that develops in the steady state hill as it isovolumetrically weathers. In these steady state models, porosity develops as a function of q_y, reactive mineral content (ϕ^0_{ab}), and protolith porosity ($\phi_{initial}$) to allow the weathering advance rate W to equal the erosion rate E. Because we are assuming isovolumetric weathering, as q_y and η_{max} increase, the porosity, ϕ, of material remaining behind that is eroding also increases: $\phi = \phi_{initial} + \phi^0_{ab}(1 - \frac{V^0_{kao}}{2V^0_{ab}})\eta \approx \phi_{initial} + 0.5\phi^0_{ab}\eta$. Here, V^0_{kao} and $V^0_{ab}$are the specific volumes of the minerals.

Just as E controls the slope of the hill surface, q_y controls the slope of another emergent property, the surface of the (unweathered) protolith. At high q_y, the slope of the protolith surface becomes shallower (Fig. 3). This trait is exemplified in the weathering of schistose rocks in the Piedmont of the eastern USA. (Pavich et al., 1989). These rocks show evidence of deep infiltration (high q_y), including deep alteration along foliations, schistosity, and cleavage (Nutter, 1969). Consistent with the prediction of a shallow protolith slope, Pavich et al. showed a schematic of a hill on metapelite that appears 100% weathered (Pavich et al., 1989). An example of weathering schist from the Piedmont is discussed in Section 8.

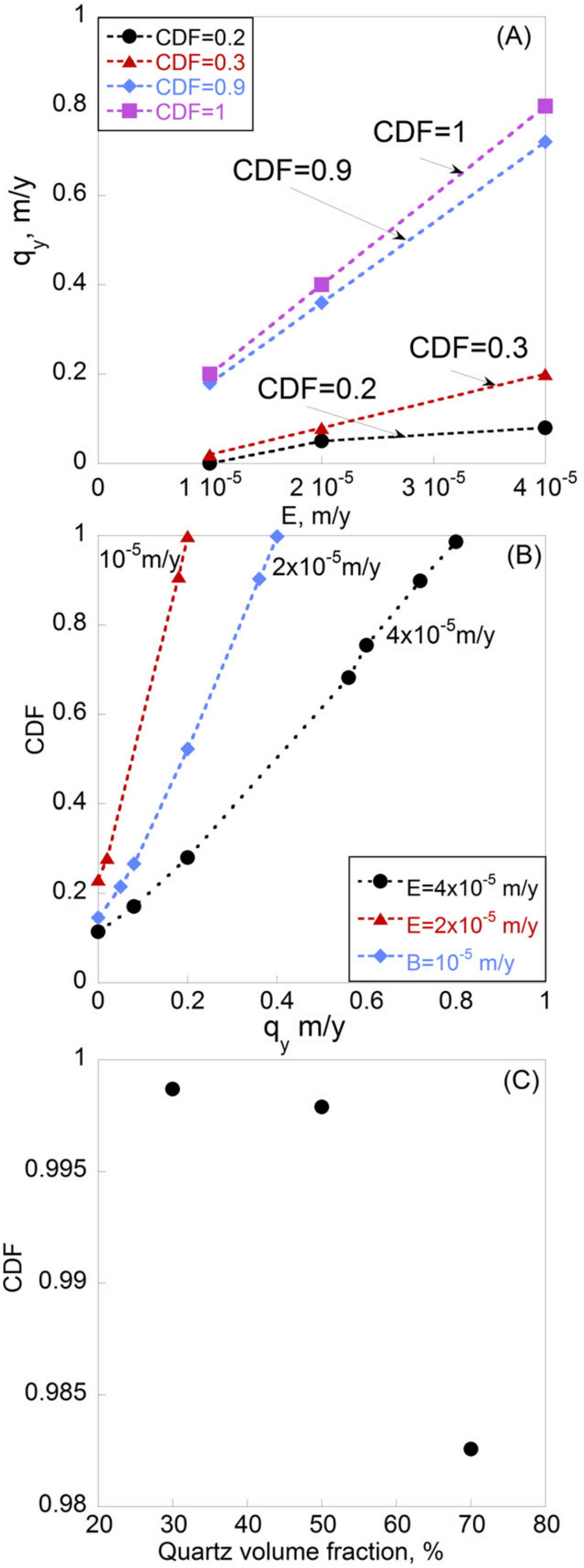

Fig. 4. Summary of calculations shown in Fig. 3: (A) contours of chemical depletion fraction, CDF, calculated for the simulated hills in Fig. 3 on a graph of vertical Darcy velocity q_y versus erosion rate E; (B) contours of E on a graph of CDF versus q_y. Additional calculations described in text (see also Fig. 5) are shown in (C): calculated model CDF values are plotted versus quartz volume fraction in the protolith. In this context, CDF is the fraction of the hill that was removed by solubilization reactions (the fraction of total denudation that was removed by chemical weathering (see supplementary information)). For panel (C), $E = 2 \cdot 10^{-5}$ m y^{-1}, $q_y = 0.4$ m y^{-1}.

At high q_y, L&B models also show that the depth interval over which chemical reaction occurs (the reaction front where $0 < \eta < 1$) becomes thicker. This reaction front thickness along the hillslope is thus another emergent property of the steady state system. Once q_y increases to the point that $\eta_{max} = 1$ (Fig. 3E), increasing q_y no longer can result in an increase in porosity as discussed in the last paragraph. Instead, for the hill to achieve steady state, an increase in q_y only results in thicker regolith at ridge and at valley.

So far, we held the composition constant at 50% quartz in the model used to generate Fig. 3. We therefore next explore the effect of % quartz in the L&B model under conditions of constant E and q_y (Figs. 4C, 5). As % quartz increases, the ridgetop regolith and the reaction front thicken. These simulations are consistent with observations within the Virginia Piedmont (Pavich et al., 1989). In that setting, regolith depth under interfluves increases with the quartz content on rocks of different lithology as shown in Fig. 6. In another example, the regolith and the reaction fronts on granitic rock in Panola Mountain, Georgia (28% quartz) are thinner than observed at Davis Run, Virginia (41% quartz), USA (White et al., 2001; Bazilevskaya et al., 2013). Both of these systems are weathering in the Piedmont with roughly similar erosion and precipitation rates, i.e., similar E and q_y (Bacon et al., 2012). The GA and VA field settings demonstrate that reaction front and regolith thicknesses are emergent properties of hills.

As discussed above, the L&B model is based on the assumption that rates of advection are everywhere the same and everywhere vertical. This latter assumption is only roughly true because permeability changes significantly within rock material inside hills and zones of lateral flow are common (Pain and Ollier, 1996). In fact, White et al. (2001) argued that much of the permeability contrast inside hills developed on granitic bedrock arises because of mineral reaction. Specifically, changes in porosity and permeability may be especially important at reaction fronts where mineral abundances vary. Such fronts can be stacked or nested when considered in 1D or 2D respectively (Brantley et al., 2011; Brantley et al., 2013a). We explore reaction fronts in hills (Figs. 1, 2) in the next section, and then we explore how they may be related to water flow and water tables in the following sections.

4. Reaction fronts

4.1. The geometry of reaction fronts

Here we consider weathering profiles and reaction fronts under ridges (Fig. 2). The nature of the bottom of the front where the reaction initiates is dictated by the upward flow of solid earth materials and downward flow of meteoric waters. In particular, as rock moves upward as a result of exhumation, it fractures. For example, at ~2 km depth in granites in the northeastern USA, the average microcrack orientation transforms from vertical to horizontal as the stress state changes during exhumation (Nadan and Engelder, 2009). At shallower depths, larger sheet fractures oriented parallel to the land surface begin to open in the rock (Molnar et al., 2007; Nadan and Engelder, 2009; Lachassagne et al., 2011). As meteoric water flows through such thermoelastic and topographic cracks as well as matrix pores and tectonic microcracks, the rock material weathers and forms reaction fronts (Ollier, 1967; Fletcher et al., 2006; Ayraud et al., 2008; Navarre-Sitchler et al., 2015). Such reaction fronts can roughly mimic the land surface but they are

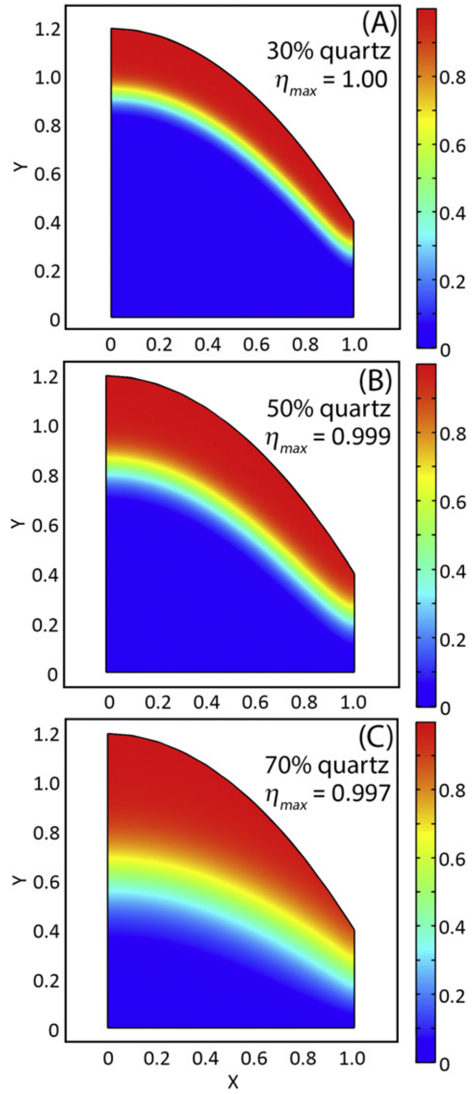

Fig. 5. The L&B model-simulated steady-state hillslopes showing the weathering extent (colored contours) as a function of quartz volume fraction in protolith, as noted. For description of contours, see Fig. 3 caption. The steady state thickness of regolith under the ridge and along the hillslope both increase as the % quartz increases. Here, the erosion rate and the vertical Darcy velocity were held constant at $E = 2\cdot 10^{-5}$ m y^{-1}, $q_y = 0.4$ m y^{-1}. For all cases here and Figs. 3 and 4, the intrinsic kinetic constant was set as $k_{ab} = 3.87\cdot 10^{-10}$ mol m^{-2} s^{-1}. The effective constant was calculated from the equation, $k = 2k_{ab}s_{ab}\phi^0_{ab}\Psi$ (Lebedeva et al., 2010). Note that k depends on ϕ^0_{ab}: (A) $k = 1.95\cdot 10^{-8}$ s^{-1}; (B) $k = 1.3\cdot 10^{-8}$ s^{-1} (also for Figs. 3 and 5); and (C) $k = 0.65\cdot 10^{-8}$ s^{-1}. In later L&B papers (Lebedeva and Brantley, 2013; Lebedeva et al., 2010) the factor ϕ^0_{ab} is included in Ψ and the effective constant is written as $k = 2k_{ab}s_{ab}\Psi$. Parameters are: (A) $\phi^0_{ab} = 0.6$, $\phi_{qtz} = 0.3$, $\phi = 0.1$, CDF = 0.999, (B) $\phi^0_{ab} = 0.4$, $\phi_{qtz} = 0.5$, $\phi = 0.1$, CDF = 0.998; (C) $\phi^0_{ab} = 0.2$, $\phi_{qtz} = 0.7$, $\phi = 0.1$, CDF = 0.982. The specific surface area $s_{ab} = 3.5\times 10^4$ m^2 m^{-3} and the correction factor $\Psi = 1.2\times 10^{-3}$ m^3 mol^{-1}.

also affected by physical heterogeneities such as veins, fractures, and faults, so that the reaction fronts are rough at all scales (Navarre-Sitchler and Brantley, 2007; Navarre-Sitchler et al., 2013). For example, where fracture zones allow deeper infiltration (Welch and Allen, 2014), reaction fronts are deeper compared to the surrounding unfractured zones (Dewandel et al., 2006; Drake et al., 2009).

For an upland system developed on one rock type, several reaction fronts can nest one within the other. Each front is a curved surface that somewhat parallels the landscape; however, the relief of deeper reaction fronts is generally lower than that of shallower fronts (Chigira, 1990; Chigira and Sone, 1991; Chigira and Oyama, 1999; Taylor and Eggleton, 2001; Ayraud et al., 2008; Drake et al., 2009; Brantley et al., 2013a). While reaction fronts tend to be nested under convex-up hilltops, the fronts may cross under valleys where water flow paths merge (Chigira and Oyama, 1999; Brantley et al., 2013a).

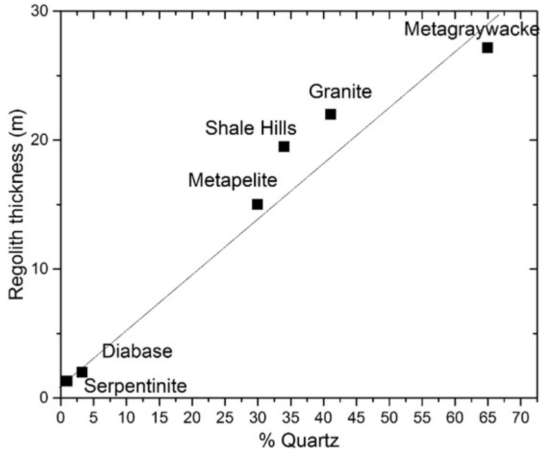

Fig. 6. Summary compilation of thickness of ridgetop regolith for case studies discussed in this paper and for other lithologies in the VA Piedmont (Pavich et al., 1989). The systems are all assumed to be experiencing the same rates of uplift and, given the long exposure times, similar rates of erosion. The one exception is the symbol for Shale Hills, where the plotted value derives from an estimate for ridges in the Susquehanna Shale Hills Critical Zone Observatory. The erosion rate of that system is higher than the rate estimated for the Piedmont (see text). This figure shows that regolith is thicker on rocks with a lower fraction of soluble mineral (i.e., higher quartz content).

The exact geometry of such reaction fronts is unknown. However, geophysical tools can be used to assess the depths of weathering and fracturing because rock properties change due to these processes. For example, weathering and fracturing can cause the seismic velocities of rock material to decrease (Holbrook et al., 2014) and mapping of such low-velocity zones can therefore sometimes be related to fracture zones or reaction fronts. Under hills characterized by relief of tens of meters in the South Carolina and Maryland Piedmont, for example, the seismic low-velocity zone extends to tens of meters under ridges but to shallower depths under valleys (St. Clair et al., 2015). This so-called *bowtie or pinched topography*—deep low-velocity zones under hills combined with shallow low-velocity zones under channels—was attributed by St. Clair et al. (2015) to opening of fractures and to weathering under the hillform that occurred in the presence of the compressive state of stress in the Piedmont.

More such geophysical surveys are needed to understand the explanations for such subsurface properties. For example, water flow could be dominantly downward under ridges and could drive net dissolution and mineral alteration, resulting in slower seismic velocities. Minerals generally dissolve in downflowing water along flowlines as long as reactants have not been 100% consumed and the water has not yet equilibrated. In high-relief valley-ridge systems, dissolution and water flow could occur even deeper than the elevation of the nearby channel, resulting in a pinched topography such as that observed by St. Clair et al. (2015). Indeed, once acids and oxidants are consumed, minerals can precipitate or re-crystallize. Thus, as the water flows upward from beneath the ridge into the valley, it could drive net mineral precipitation in relatively unaltered bedrock, resulting in faster seismic velocities under the valley in some cases. In addition, if carbon dioxide degasses during upflow, it can raise pH and cause mineral precipitation (Brantley et al., 2013a). Such flow patterns have been discussed in the literature (Tóth, 1970).

Little is known about the complexity of such layers and flowpaths inside hills. In the next sections, we explore some very simple ideas about reaction fronts, water flowlines, and their implications. We emphasize reaction fronts under convex-upward hillslopes developed on a single lithology near the upper parts of catchments where the fronts are likely to be nested, mimicking surface topography. Thus our discussion does not treat pinched topographies where weathering may occur deeper under the ridge than under the nearby channel. Our discussion focusses on a sequence of reactions that can create identifiable layers in regolith under a ridge: the profile-initiating reaction, the major porosity-initiating reaction, and the soil-initiating reaction.

4.2. The profile-initiating reaction: oxidation or acid neutralization

As rock material advects upward under a hill, it begins to weather as its mineral surfaces interact with water and atmospheric gases. We use the term *profile-initiating mineral* for the most soluble mineral that first weathers at depth in the protolith to form weathered rock (Brantley and White, 2009). In Fig. 1, the difference between the depth where the profile-initiating mineral first reacts under the hillcrest and the elevation of the associated channel is noted as ΔB_2. Thus, the relief of the protolith surface is noted as ΔB_2 (Fig. 1).

This deepest reaction is often an oxidation reaction, especially in quartzo-feldspathic rocks. This is because O_2 generally is not consumed as fast as CO_2 during reaction of a felsic rock. For example, Brantley et al. (2013b) observed that oxidation was the deepest reaction in a felsic Fe-poor rock in the Virginia Piedmont, but that acid-driven dissolution was the deepest reaction on a nearby mafic, Fe-rich rock.

The effect of rock composition on O_2 and CO_2 consumption is related to the ratio, R^o, of O_2-consuming oxides to CO_2-consuming base cation oxides in the rock. The ratio R^o can be calculated (Holland and Zbinden, 1988; Feakes et al., 1989) using the expression, $R^o = M^o_{FeO}/(8(M_{Na_2O}{}^o + M_{K_2O}{}^o + M^o_{MgO} + M^o_{CaO}))$. Here, FeO is assumed to be the dominant redox-active oxide and M^o_{oxide} is the moles oxide per kilogram protolith. Reaction stoichiometry dictates that 0.25 mol of O_2 are consumed per mole of reacted FeO and 2 mol of CO_2 per mole of solubilized base cation oxide. The R^o value, the capacity of the protolith to consume oxygen ratioed to its capacity to consume acid, tends to be larger for mafic rocks than felsic rocks. For example, the R^o for a typical diabase (0.04) is larger than for a granite (0.02) because diabase has a high content of Fe(II) compared to base cation oxides. Thus, for some mole ratios of CO_2:O_2 in the soil atmosphere, a gas mixture will become depleted in O_2 before CO_2 on a mafic rock but not on a felsic rock. Consistent with this, acid dissolution has been documented deeper on a diabase weathering in the VA Piedmont than oxidation whereas the opposite was observed on a nearby granite (Bazilevskaya et al., 2013). Of course, the rock composition (R^o) is only one part of the control on the profile-initiating reaction: also of importance is the composition of the soil atmosphere and the biotic controls on O_2 consumption and CO_2 generation in the soil (Brantley et al., 2013b).

4.3. The importance of pyrite

The R^o as described above is essentially a mass balance on mineral components in a rock that consume O_2 vs. CO_2. To calculate the relative depths of oxidation and acid-driven dissolution in a rock containing significant pyrite and carbonate, the R^o as defined above is inadequate. For rocks with sufficient pyrite and calcite, the formula for R^o can be modified (Feakes et al., 1989; Brantley et al., 2013a): $R^o = (0.25M^o_{FeO} + 3.75M^o_{FeS2})/(2(M_{Na_2O}{}^o + M_{K_2O}{}^o + M^o_{MgO} + M^o_{CaO}) + M^o_{CaO(cc)})$. Here, $M^o_{CaO(cc)}$ and M^o_{FeS2} are the moles of calcite and pyrite per kilogram of protolith, respectively. This equation takes into account that one mole of pyrite (FeS_2) consumes 3.75 mol of O_2, and one mole of $CaCO_3$ consumes one mole of CO_2 during dissolution.

However, important aspects of pyrite's reactivity that are not incorporated in R^o are that pyrite oxidation releases the strong mineral acid H_2SO_4 and that oxidation can be autocatalytic. When pyrite is abundant, therefore, the released sulfuric acid may dissolve minerals and cause significant dissolution near the oxidation zone (Chigira and Oyama, 1999). Such H_2SO_4-driven dissolution can be important at the pedon, watershed, and global scales (Lichtner and Waber, 1992; Calmels et al., 2007; Torres et al., 2014).

In some rocks with high pyrite content, enough H_2SO_4 can be generated to develop significant permeability at depth (Ayraud et al., 2008). Zones of such high permeability associated with pyrite oxidation are often found near the water table. This is likely because the water table demarcates a gradient in O_2 concentration dividing the vadose zone, where gas migrates quickly, from the water-saturated phreatic zone, where gas migrates slowly (Bornstein et al., 1980). However, pyrite is also sometimes observed to have been oxidatively dissolved from rock materials recovered from beneath the water table (Ayraud et al., 2008; Brantley et al., 2013a). Such oxidation may occur when oxygenated fluids are transported beneath the water table (Sullivan et al., in press). Another explanation could be that the water table was lower in the past. This may be particularly applicable in mid-latitude North America, where the last 2000 years have been substantially wetter than the previous 100,000 years (Shuman and Marsicek, 2016).

Pyrite may also oxidize beneath the water table because of oxidants other than oxygen. For example, many bacteria associated with pyrite oxidation can use nitrate rather than oxygen as the electron acceptor and nitrate is sometimes advected beneath the water table (Ayraud et al., 2008). In addition, the Fe^{3+} that is released to solution by pyrite oxidation can itself act as an oxidant (Nordstrom, 2000). Pyrite oxidation is thus autocatalytic because it produces a product (aqueous Fe^{3+}) that is also a reactant. Rocks rich in pyrite therefore can develop zones of enhanced secondary permeability when an oxidant (e.g., O_2, NO_3^-, Fe^{3+}) is available at high concentration.

4.4. Major porosity-initiating and soil-initiating reactions

As rock material advects upward above the depth of the profile-initiating reaction where the most soluble mineral reacts, the moderately soluble minerals eventually begin to dissolve and create porosity and permeability. When this next reaction involves a more abundant mineral such as feldspar that reacts isovolumetrically to create porosity, we term the reaction the *major porosity-initiating reaction*. In some cases this front demarcates formation of saprolite.

At an even higher elevation, ΔB_1, above the nearest channel (Fig. 1), a *soil-initiating reaction* demarcates the bottom of massive soil or soil. The soil-initiation reaction generally involves another abundant mineral. Dissolution of this mineral causes further disaggregation and clay formation in a zone of intense biological processing where weathering eventually becomes nonisovolumetric. This soil-initiating mineral has lower solubility than the major porosity- or profile-initiating minerals.

Notably, these reactions can cause large changes in porosity and permeability. For example, the profile-initiating reaction may *cause* the transformation from bedrock to weathered rock, the major porosity-initiating reaction may *cause* the transformation from weathered rock to saprolite, or the soil-initiating reaction may *cause* the transformation from saprolite to massive soil. In these cases the reactions may cause large enough porosity and permeability changes that water flow paths transition from vertical to horizontal (Balashov et al., 1999; Brantley et al., 2013b). Alternatively, some other physical, hydrological, or biological mechanism may cause the transformation from bedrock to weathered rock or weathered rock to saprolite or saprolite to soil; in such cases, the reactions may simply be co-located at the depths where that phenomenon is important. Regardless, we argue that the elemental depth profiles can nonetheless yield information about flow patterns and the cumulative flows of water, as explored in Section 6. First, however, we summarize in the next section the three case examples showing stacked reaction fronts from the mid-Atlantic region of the eastern USA. Evidence suggests that these systems are near or approaching steady state conditions (Pavich et al., 1989; West et al., 2013).

5. Case studies

5.1. Virginia Piedmont diabase and granite

The first two cases are diabase and granitic rocks weathering at ridgetop positions in Virginia (Pavich, 1986; Pavich et al., 1989; White et al., 2001). The two lithologies have an initial porosity of about 2–3% and are eroding at rates that are equivalent within error (±30%): $4.5 < E < 13$ m My^{-1} (Pavich et al., 1985; Pavich et al., 1989; Price et al., 2008; Portenga and Bierman, 2011; Bacon et al., 2012). The ridgetops have weathered to form residual soils on bedrock in the Piedmont, a physiographic province characterized by low relief ranging in elevation from 90 to 200 masl. The temperate climate is characterized by a MAP of ~1040 mm y^{-1}.

Hills in the Piedmont are close to geomorphological equilibrium given the long exposure time and low erosion rates (Pavich et al., 1989). This is shown by data in Table S1 (Supplementary information) which summarizes the averages for the slopes of hills in the region on the different lithologies. The slopes in the table were approximated as r/L for 10 hills on diabase and granite in the VA Piedmont. Here, r is the relief of the hill and L is the distance from hillcrest to the nearest channel head (Fig. 1). The values for the slopes measured from the hillcrest down to the channel head are equal within error (0.04 ± 0.02 vs. 0.05 ± 0.01, respectively), consistent with the similar erosion rates, as discussed for Fig. 3 or Eq. 6 in Section 3.

The diabase profile discussed here is from a borehole in the Late Triassic Manassas sill complex (Smith et al., 1975). The rock contains about 3 vol.% quartz, 54 vol.% plagioclase feldspar, and 36 vol.% pyroxene (augite) with minor hornblende, ilmenite, magnetite, pyrite, and occasional reports of trace biotite. In optical microscopy, the augite shows ferrous-rich and -poor lamellae (Bazilevskaya et al., 2013; Bazilevskaya et al., 2014). The regolith thickness at the ridgetop is 2 m (Fig. 2).

The granitic rock is a metamorphosed light-gray muscovite-biotite monzogranite (Lonsdale, 1927; Drake and Froelich, 1977) belonging to the Cambro-Ordovician Occoquan Formation. It contains about 41 vol.% quartz, 52 vol.% feldspar, and 7 vol.% mica, including biotite and muscovite (Bazilevskaya et al., 2013). The protolith is a two-feldspar granite (i.e., plagioclase and alkali feldspar) and includes trace zircon, pyrite, and magnetite (White et al., 2001). The primary quartz and feldspar mineral grains can exceed 6 mm (Lonsdale, 1927). The regolith thickness under the ridgetop, measured down to protolith, is ~22 m (Fig. 2).

The diabase has a high FeO content compared to base cation oxides ($R^o = 0.04$); and consistent with the discussion in the last section, the profile initiation reaction is acid-promoted dissolution rather than oxidation. Specifically, the first reaction is dissolution of Fe(II)-containing augitic pyroxene without precipitation of ferric oxide. Lamellae of this composition in the pyroxene are observed under transmission electron microscopy to have dissolved to a small extent in thin sections from 2 m depth in the weathered-rock zone (Bazilevskaya et al., 2014). Such solubilization and removal of Fe typically occurs in the absence of O_2. Solubilization of this profile-initiating mineral, ferrous pyroxene, has therefore been attributed to consumption of O_2 higher in the rock consistent with the high ferrous content (large R^o value). Where O_2 is still present higher in the profile (above ~1 m), the Fe in the pyroxene was dissolved and reprecipitated as Fe oxide (Bazilevskaya et al., 2013; Bazilevskaya et al., 2014). In addition, pyrite is generally missing from the rock down to about 1.8 m depth.

In contrast, the deepest profile-initiating reactions in the ferrous iron-poor granite is oxidation of biotite and oxidative dissolution of pyrite (Bazilevskaya et al., 2014). The relatively thin oxidation depth interval is also marked by loss of K^+. Biotite loses this cation to maintain charge balance as Fe(II) is oxidized to Fe(III). Thus, we infer that O_2 remains present at relatively high concentrations to significant depths on this lithology (Brantley et al., 2013b; Navarre-Sitchler et al., 2015). Biotite and pyrite are oxidized at a depth somewhere near 20 m, defining the weathered/unweathered rock interface (Bazilevskaya et al., 2013; Bazilevskaya et al., 2014).

Above the profile-initiating reactions on the diabase (ferrous pyroxene dissolution) and the granite (biotite oxidation), the next minerals to react are calcic pyroxene and plagioclase feldspar, respectively. These reactions, which proceed to 100% completion, mark the transformation of weathered rock to saprolite (Figs. 2A,B). The nature of these major porosity-initiating reaction fronts are different in the two rocks, however. The reaction front for calcic augite in the diabase (Fig. 2A) is only a few tens of centimeters in thickness (Bazilevskaya et al., 2013; Brantley et al., 2013b; Bazilevskaya et al., 2014). In contrast, the reaction front for plagioclase in the granite is much wider (9–10 m, Fig. 2B). Bazilevskaya et al. (2013) used model simulations to argue that the wider reaction front for plagioclase on the granite was caused by a larger advection velocity of water through the front compared to the pyroxene front on the diabase (see the wider fronts in Fig. 3E vs. 3H).

The final reactions on the two lithologies are the soil initiation reactions: dissolution of plagioclase in the diabase and alkali-rich minerals in the granite. All these important reactions in the diabase—the reaction fronts for profile initiation (ferrous pyroxene), major porosity initiation (calcic pyroxene), and soil initiation (plagioclase)—are located within centimeters of one another (Fig. 2B). In contrast, the alkali-rich minerals dissolve in the upper 3 m of the granite, tens of meters above the deeper-dissolving plagioclase (Fig. 2).

5.2. Rose Hill shale

The third example is weathering of Rose Hill shale in the Valley and Ridge Physiographic province in Pennsylvania in the Susquehanna Shale Hills Critical Zone Observatory (Fig. 2). Based on isotopic measurements, the rate of erosion of the Shale Hills catchment, ~30 m/My, is several times greater than that of the rocks of the Piedmont (West et al., 2014). Consistent with this higher erosion rate, the slope, r/L, equals 0.19 for the Rose Hill shale, significantly higher than the shallow slopes exhibited by the hills in the Piedmont on the more competent diabase and granite lithologies (0.04 to 0.05). This higher slope is consistent with Eq. (6) because of the faster erosion. At Shale Hills, West et al. showed that the rate of erosive loss of soil is within error of the rate of production of soil at the ridgetops. Therefore, like the Piedmont, the weathering advance rate under the ridgetops is considered here to be roughly equal to the erosion rate.

In the Rose Hill shale, pyrite oxidation and carbonate dissolution are the deepest reactions inferred to occur beneath the ridge and it is difficult based on sample recovery to determine which reaction occurs deeper (Brantley et al., 2013a). Pyrite is depleted to depths of 23 m beneath the northern ridge, to 16 m beneath the southern ridge closer to the outlet of the watershed, and to 8 or 9 m beneath the channel (Jin et al., 2011; Brantley et al., 2013a; Sullivan et al., in press). Oxidation of the trace mineral pyrite comprises a very thin (<1 m) reaction front (Fig. 2). Under the ridge, the pyrite front is coincident with the zone of water table variation; but under the valley, the front is deeper than this zone. Pyrite is assumed here to be the profile-initiating reaction in the shale.

Partly because of acid released during pyrite oxidation and partly because of carbonic acid, carbonate minerals have also dissolved to a depth of ~23 m beneath the northern ridge (Brantley et al., 2013a) and have a reaction front thickness ≤ 3 m. Under the valley, carbonate is depleted only to a depth of about 2 m, roughly coincident with the water table. Jin et al. (2011) called the carbonate-free material *saprock* because it maintains much of the physical character of bedrock. For the shale, we define carbonate dissolution as the major porosity-initiating reaction, although it did not disaggregate the rock into saprolite and it may even initiate deeper than pyrite oxidation, perhaps because H_2SO_4 diffused downward.

Within the saprock near the pyrite and carbonate reaction fronts, oxidation of chlorite also begins, releasing Mg to solution as the mineral transforms to vermiculite (Fig. 2C). Under the ridge, this oxidation begins near the water table and continues upward. Under the valley, this oxidation begins at 8–9 m depth. Very little change in physical character of the saprock has been observed to correlate with chlorite oxidation other than occasional microcracking.

Finally, in a heavily fractured zone of altered rock that characterizes the upper ~6 m throughout the catchment, illite dissolution initiates and eventually disaggregates the rock to form augerable soil. Illite dissolution is thus defined here as the soil-initiating reaction. The fracture zone has been attributed to frost-related processes during the late Pleistocene and Last Glacial Maximum (Jin et al., 2010).

6. Depth, thickness, and spacing of reaction fronts at ridgetops

As described in the last section, the depth, thickness, and spacing of many of the reaction fronts were observed to be larger on the quartzofeldspathic examples (granite, shale) than on the mafic rock. Although the number of case studies is small, such patterns have been noted elsewhere as well (Cleaves et al., 1970; Rice et al., 1985; Pavich et al., 1989; Buol and Weed, 1991; Nesbitt and Markovics, 1997; White et al., 1998; White et al., 2001; Anderson et al., 2002; White et al., 2002; Hausrath et al., 2011; Bazilevskaya et al., 2013; Behrens et al., 2015; Navarre-Sitchler et al., 2015).

Bazilevskaya et al. (2013) explained the observation of thicker regolith on granitic as opposed to mafic rocks by a four-fold argument related to the production of weathering-induced fractures at the base of the weathering profile: (i) the profile-initiating reaction tends to be oxidation rather than acid-promoted dissolution on felsic rocks because of the low R^o; (ii) oxidation is often marked by an increase in volume that drives cracking (e.g., Fletcher et al., 2006); (iii) cracking promotes advective transport; and (iv) solute transport by advection tends to thicken regolith (as well as widen reaction fronts) (Brantley and Lebedeva, 2011). Biotite oxidation may be an especially important reaction in cracking felsic rocks (Eggler et al., 1969; Van Tassel and Grant, 1980; Nesbitt and Markovics, 1997; Fletcher et al., 2006; Buss et al., 2008; Lachassagne et al., 2011). However, reactions of minerals such as pyroxene have also been associated with cracking (Jamtveit and Hammer, 2012; Behrens et al., 2015).

The key point here is these oxidation reactions are like pyrite oxidation in that they are autocatalytic: they produce a reaction product (in this case, newly cracked surface area) that acts as a reactant that promotes further chemical reaction. Such autocatalysis thus creates an environment that can drive continued fracturing and deeper weathering penetration into protolith. In fact, subhorizontal fracture sets that are often tens of meters in thickness and highly friable are observed in the upper meters of crystalline bedrock at the base of many weathering profiles at depths to 100–200 m, and some argue that these fractures are caused by the weathering itself (Jones, 1985; Dewandel et al., 2006; Legout et al., 2007; Lachassagne et al., 2011; Welch and Allen, 2014). Some researchers argue that alternative drivers for fracturing such as tectonic activity or topographic readjustment cannot explain many of the observations of such deep fractured zones on crystalline rock (Lachassagne et al., 2011). These deep fissured zones have been described to sometimes be roughly coincident with the water table or sometimes to lie well below the water table (e.g. Jones, 1985). Examples of fissured rock layers in the literature are generally derived from felsic rocks.

In addition to the formation of a fissured zone at the top of felsic bedrock under weathering profiles, another reason for enhanced advection through reaction fronts on felsic rocks is that the porosity of these rocks is propped open during weathering because they have higher contents of quartz (Figs. 5, 6) and intergrowths of K-containing mica and quartz (Pavich et al., 1989). Without quartz and K mica, regolith may be thinner on mafic rocks. In addition, smectitic clays form more readily on mafic rocks because of the high Ca and Mg content, and these clays can expand and plug porosity, restricting water influx (Rice et al., 1985; Pavich et al., 1989; Buol and Weed, 1991). We argue that these tendencies all lead to thicker regolith and wider reaction fronts on quartzo-feldspathic as compared to mafic rocks (when all else is held equal).

The final important observation from the case studies is that the reaction fronts are spaced more widely in the felsic as compared to the mafic rocks (Fig. 2). Numerical models of granitic weathering have been used to investigate such spacing (Moore et al., 2012; Brantley et al., 2013b). Moore et al. concluded that the separation between the plagioclase and potassium feldspar reaction fronts was larger in simulations that were maintained unsaturated and open to CO_2. In the presence of lower pH and high CO_2 concentrations under unsaturated conditions, feldspar weathering was maintained far from equilibrium, and reaction fronts for alkali and plagioclase feldspars became separated. In addition, Brantley et al. (2013b) modelled the effect of both CO_2 and O_2 on weathering and concluded that lower CO_2 and higher O_2 in the soil atmosphere, such as expected at the base of a felsic rock with low R^o, results in separation of the acid and oxygen consumption fronts. In contrast, for a rock like the diabase where the soil atmosphere evolves at depth to relatively high CO_2 and low O_2, modelled fronts were observed to almost co-locate, as observed in the diabase (Fig. 2).

7. Conceptual model for two-layer lateral flow inside hills

Although the L & B model requires that water flows predominantly downward in the unsaturated zone, water also flows laterally in hills (Pain and Ollier, 1996; Tague and Grant, 2004; Katsura et al., 2008). In hills developed on crystalline rocks, for example, lateral water flow is especially common in the depth intervals of fluctuation of the water table where chemical reactions are prevalent and where it is common to observe a highly fractured and friable zone of weathered rock as described in the last section (Legout et al., 2007; Ayraud et al., 2008). Biogeochemical reactions are localized in this zone because (i) O_2 and CO_2 are entrained into the water as the water table fluctuates; (ii) O_2 or other oxidants drive oxidation of minerals such as pyrite and biotite in this zone (Taylor and Eggleton, 2001; Ayraud et al., 2008; Lachassagne et al., 2011), and (iii) water chemistry changes rapidly and frequently, driving dissolution (Legout et al., 2007).

Lateral flow in hills is not always observed to be confined to the zone of the fluctuating regional water table however. In fact, anywhere a high-permeability surface layer overlies a low-permeability sublayer, water can flow laterally (e.g., Katsura et al., 2008) as long as the permeability contrasts are about an order of magnitude (Hopp and McDonnell, 2009). Such flow has been reported in shales, conglomerates, granites, volcanics, schists, and other metasedimentary rocks (Cleaves et al., 1970; McDonnell, 1990; McGlynn and McDonnell, 2003; Peters et al., 2003; Tague and Grant, 2004; Ayraud et al., 2008; Katsura et al., 2008; Graham et al., 2010; McGuire and McDonnell, 2010; van Meerveld et al., 2015; Sullivan et al., in press).

Here the term *interflow* is used to refer to such lateral flow occurring high in a hill. This term is used to differentiate it from lateral flow deeper within the hill, referred to here as *groundwater flow*. Sometimes this interflow may be perched. In other cases, this high-elevation lateral flow may occur because of a very high transient water table. Whether interflow is perched or not, this lateral water flow is important in hills in addition to lateral flow in the deeper zone. In the well-studied Panola granite in Georgia (USA), for example, a well-defined low-permeability layer located at shallow depths high in the hill allows lateral flow of water to the channel after rain events; however, water also flows laterally at a deeper boundary layer between weathered and unweathered rock (van Meerveld et al., 2015). In crystalline felsic rocks such as the Panola granite, such a deep zone of lateral flow is expected as described in the last section, because such aquifers commonly have a high-permeability fissured and friable weathered rock layer situated between the overlying saprolite and the underlying protolith (Jones, 1985). This deep fissured layer might be the layer where spheroidal weathering begins due to biotite oxidation as observed in some systems (Buss et al., 2008). In this paper, the upper flow is referred to as interflow and the lower flow as groundwater flow. We argue that two such zones are likely where reaction fronts have separated over meters or tens of meters, such as for the granite and shale in Fig. 2. In contrast, on massive mafic rocks where reaction fronts do not separate, two zones of lateral flow are not likely to develop (Fig. 2A).

We have not developed a numerical treatment of complete geochemical regolith evolution in hills with vertical and lateral fluid flow. In Figs. 3–5, for example, the Darcy velocities were held constant and vertical everywhere. However, because some simulations (see Fig. 3A) show that hills can have near-linear slopes, we instead explore the flow patterns for a planar hillslope simply by considering what mass balance might look like for a steady state (Fig. 7). The linear hill is assumed to be characterized by reaction fronts that record fluid flows at that depth.

We start with a 1D conceptualization (Fig. 8). Net water flow downward occurs above the upper reaction front (RF_1) defined as the soil-initiating reaction. The zone above RF_1 is also the location of interflow. At greater depths, a second reaction delineates RF_2 and the location of groundwater flow. As we have discussed, for quartzo-feldspathic rocks, RF_2 is likely to be near the oxidation front. RF_1 is the front where CO_2 consumption initiates and the organic acids are largely consumed. However, CO_2 is also consumed in reactions between RF_1 and RF_2. In the diagram, the bottom of each front is labelled as RF_1 or RF_2 and the concentration of the reacting mineral is assumed to be identical to that of protolith at that point.

Intermittently, a zone of water saturation occurs above RF_1, varying up and down within the hachured zone. This is the zone of occasional interflow and is labelled Q_{int} and is colored on Figs. 7 and 8. Likewise, the onset of oxidation at RF_2 marks the bottom of the major porosity-initiating reaction and is often coincident with the interface between weathered rock and protolith. The lower colored zone sitting above RF_2 shows the zone of variation in elevation of the regional water table. This is the zone we term groundwater flow, Q_{gw}.

For Q_{int} at RF_1 and Q_{gw} at RF_2, the thicknesses of the flow zones (H_{int} and H_{gw} respectively; Fig. 7) are assumed to be coincident with the thicknesses of the variations of the water table for interflow and groundwater flow, respectively. These depth intervals are considered to be zones of marked contrast in permeability that are caused in at least some cases by biogeochemical reactions. In the zones of water table variation, lateral flow occurs, biogeochemical reactions are relatively fast, removal of material is relatively fast, and the extent of weathering is high. The upper reaction front may also sometimes overlie a zone of intense precipitation or illuviation of clay minerals that occlude permeability.

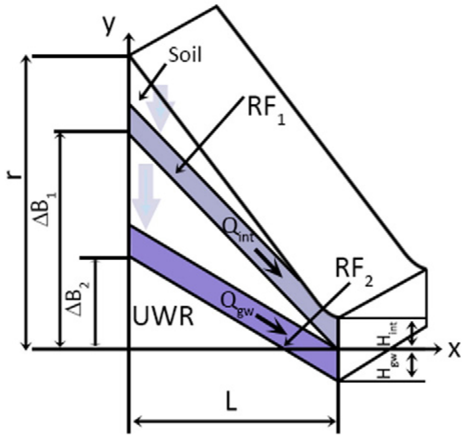

Fig. 7. A conceptual model for a hill with two layers of lateral water flow (see also Fig. 1 where some variables are defined). The upper layer is soil and the bottom layer is unweathered rock (UWR). RF_1 and RF_2 are the bottom of the upper and lower reaction fronts, respectively, as described in the text. These fronts are co-localized with zones of water table fluctuation for interflow and groundwater flow, respectively. H_{int} and H_{gw} are the depth intervals of water table fluctuation or, alternately, thicknesses of the high-permeability flow layers; these layers are characterized by hydraulic conductivities K_{int} and K_{gw}, for the interflow and groundwater flow zones, respectively. The semitransparent vertical arrows indicate the vertical flow of water in the unsaturated zone between land surface and interflow and between interflow and groundwater flow zones.

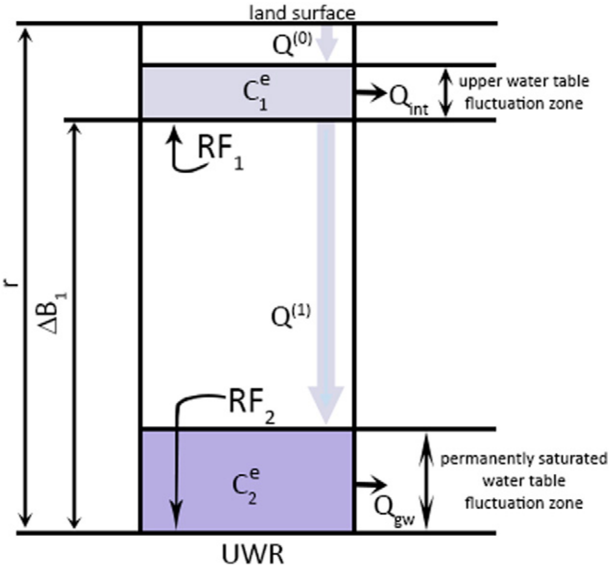

Fig. 8. The weathering domain of the two-layer lateral-flow hill model (Fig. 7) depicted in 1D. In reality, all horizontal lines are slightly inclined so that this is a parallelogram with sides parallel to a hillslope. The angle of the hillslope is assumed to be small so that the rectangle is a reasonable approximation of this domain. The soil surface moves down at a constant erosion rate and is considered equal to the weathering advance rate W. $Q^{(0)}$ and $Q^{(1)}$ represent water flow in the unsaturated zone between land surface and the upper interflow zone, or between the interflow and groundwater flow zones, respectively. Lateral flow could occur anywhere a permeability contrast is large enough to allow transient saturation; however, lateral flow is largely localized at the upper or lower reaction fronts, i.e., RF_1 or RF_2, respectively. The dissolved concentrations of the reacting mineral at equilibrium in the interflow and groundwater flow volumes are C_1^{eq} and C_2^{eq}, respectively. The upper hachured layer is the zone of water table fluctuation for the water table at highstand or for a perched layer; the lower hachured layer is the zone of water table fluctuation of the present-day regional groundwater table or a relict fluctuation zone from a previously-deeper water table (see text). For unfractured mafic systems such as the diabase in Fig. 2, RF_1 and RF_2 are almost coincident and flow does not separate into two zones. For felsic systems or fractured systems such as the granite and shale in Fig. 2, RF_1 and RF_2 separate by meters or tens of meters: in this case the lower zone of flow is typically an oxidation zone and is marked by the intense biogeochemical reactivity of minerals such as biotite and pyrite. Some variables are defined in Figs. 1 or 7.

In contrast to the lateral flow zones, in the depth intervals well above RF_1 and between RF_1 and RF_2, water flows predominantly downward as $Q^{(0)}$ and $Q^{(1)}$, respectively (Fig. 8). We know this flow occurs because of the evidence of chemical reactions in this zone and because such reaction can only occur if water is allowed to flow. Specifically, above RF_1 in Shale Hills or in the VA granite, potassium-containing minerals have dissolved and their depletion documents the cumulative passage of water. Likewise, between RF_1 and RF_2, chlorite has oxidized and plagioclase has become depleted in Shale Hills and the VA granite, respectively. The relatively wide reaction fronts for chlorite and plagioclase in Figs. 2B,C in the shale and the granite respectively (Fig. 2) document flow through the zone above RF_2 because advective transport of solutes through a front causes front widening (Bazilevskaya et al., 2013).

7.1. The mass balance equations for a linear hill model

Figs. 1 and 8 delineate three important interfaces: land surface, RF_1, and RF_2. Between these interfaces are important zones of regolith: (i) above RF_1: massive soil + soil characterized by partial, intermittent water saturation, (ii) between RF_1 and RF_2: saprolite and weathered rock characterized by partial, intermittent water saturation; and (iii) beneath RF_2: unweathered rock characterized by continual water saturation. In this section, we seek to use element concentrations to predict the ratio of interflow to groundwater flow, Q_{int}/Q_{gw}, for hills evolving such that $E = W$ (Figs. 7, 8).

The ratio Q_{int}/Q_{gw}can be determined through water mass balance:

$$Q_p = q_p A_R = Q^{(0)} = Q_{\text{int}} + Q_{gw} \tag{7a}$$

$$Q_{gw} = Q^{(1)} \tag{7b}$$

Here q_p(m/s) is the net infiltration flux (roughly, mean annual precipitation (MAP) minus evapotranspiration (ET)), and $A_R(\text{m}^2)$ is the map-view area. The downslope fluxes can be written as (Fig. 7):

$$Q_i = q_i a_i \tag{8}$$

where q_i is the Darcy velocity ($\text{L}\,\text{T}^{-1}$) in each layer i (where i refers to subscript *int* or *gw*, respectively), and a_i is the cross-sectional area of the layer of flow to the channel.

In the upper layer ($i = int$), we assume that reactive mineral 1 dissolves to release solute 1. Concentration of solute 1 at the bottom of the reaction front (at RF_1 on Figs. 7, 8) is assumed to equal the equilibrium concentration C_1^e (kg m^{-3}). Here, concentrations are calculated per unit volume of pore fluid. Likewise, a second solute, component 2, is present at equilibrium concentration C_2^e at RF_2.

The concentrations of components 1 and 2 in the solid phase are defined at RF_1 and RF_2 per unit volume of rock: ρ_1 and $\rho_2(\text{kg m}^{-3})$, respectively. If the hill achieves a steady state, then the weathering advance rate ($\text{L}\,\text{T}^{-1}$), W, can be equated for RF_1 and RF_2:

$$A_R W \Delta\rho_1^{(1)} = C_1^{av} Q_{\text{int}} + C_1^e Q^{(1)} = C_1^{av} Q_{\text{int}} + C_1^e Q_{gw} \tag{9a}$$

$$A_R W \Delta\rho_2^{(2)} = C_2^{av} Q_{gw} \tag{9b}$$

Here, $\Delta\rho_i^{(j)}$ is loss of the ith component from the solid phase at RF_1 or RF_2 ($j = 1$ or 2, respectively), and C_i^{av} is the concentration of component i in the fluid averaged over the cross section of the subhorizontal layer j. These equations express that the mass loss of each component from the solid phase is balanced by solute transport in Q_{int} and Q_{gw}. Solutes 1 and 2 are furthermore assumed to be present in insignificant concentrations in precipitation (or, alternately, the concentrations are corrected for inputs from precipitation). For simplicity in Eqs. (9a) and (9b) we assume $C_1^{av} = C_1^e$and $C_2^{av} = C_2^e$. In other words, on average the flow removes water in equilibrium with the dissolving minerals.

One complication is that components sometimes move in the subsurface not only as solutes but also as particulates (Jin et al., 2010; Sullivan et al., in press). To account for this, we write $C_1^{av} = C_1^e + C_1^{prt} = \alpha C_1^e$. Here, $C_1^{prt}$is the concentration of component 1 moving as a particle and $\alpha \geq 1$is the correction factor that corrects the equilibrium concentration to take into account this particle transport. Using these assumptions Eqs. (9a) and (9b) are rewritten as:

$$\begin{aligned} A_R W \Delta\rho_1^{(1)} &= C_1^e(\alpha Q_{\text{int}} + Q_{gw}) && \text{(a)} \\ A_R W \Delta\rho_2^{(2)} &= C_2^e Q_{gw} && \text{(b)} \end{aligned} \tag{10}$$

This second equation emphasizes that Q_{gw}/A_R (the watershed area-normalized flux of groundwater out of the system) is an emergent property in the steady state hill: it is a function of the erosion rate which is in turn set by the uplift rate (i.e., steady state weathering rate where $E = W$). It is also affected by lithology through $\Delta\rho_2^{(2)}$, and mineral solubility (C_2^e). Although derived differently for somewhat different treatments, these equations are equivalent to equations used previously (Cleaves et al., 1970; Pavich, 1986; Cleaves, 1993; White, 2008; Brantley and White, 2009). However, interflow was not taken explicitly into account in the previous work.

Our treatment emphasizes that the most soluble minerals are removed largely at RF_2 while the more moderately soluble minerals are removed at RF_1 and the least soluble minerals are removed at the land surface. In effect, we argue that the hill evolves to remove minerals of different solubilities at different surfaces by partitioning water into vertical and horizontal flow paths. Minerals can have solubilities that differ by small numerical factors (e.g., different compositions of feldspar) or by orders of magnitude (e.g., quartz and calcite). For example, the solubility of albite, which often initiates at the oxidation front RF_2 in granite, is approximately 6×10^{-7} mol L^{-1} and the solubility of potassium feldspar, which often defines RF_1, is 3×10^{-7} mol L^{-1}. In contrast, the solubility of calcite is on the order of 6×10^{-5} mol L^{-1} (Berner, 1981). Small or large differences in solubility must be accommodated by differences in cumulative flow if a hill evolves toward the steady state condition of $E = W$.

Also notable, the soil-initiating reactions on the more felsic rocks in Fig. 2 are all potassium-containing reactions. This is at least partly because the solubility of K-containing silicates tends to be lower than that of the Na-, Mg-, and Ca-containing silicates (Berner, 1981). However, K is also a nutrient that is taken up into biota, stored for short residence times, then returned to the soil during plant degradation (Jobbagy and Jackson, 2001). This internal recycling increases the aqueous K concentration in upper regolith, decreasing the reactivity of K minerals. In this sense, biota comprise a negative feedback on the K-containing minerals, slowing the rate of loss of K and Si from the top layers because of the retention of K. Likewise, biota are largely responsible for production of CO_2, and higher values of P_{CO2} in the soil atmosphere result in greater separation of the plagioclase and potassium feldspar reaction fronts (Moore et al., 2012).

Eq. ((10) constrains the ratio we seek (where the approximation is true when particle transport is insignificant):

$$\frac{Q_{\text{int}}}{Q_{gw}} = \left(\frac{\Delta\rho_1^{(1)}}{\Delta\rho_2^{(2)}} - \frac{C_1^e}{C_2^e}\right)\frac{C_2^{av}}{C_1^{av}} = \frac{1}{\alpha}\left(\frac{\Delta\rho_1^{(1)}}{\Delta\rho_2^{(2)}}\frac{C_2^e}{C_1^e} - 1\right) \approx \left(\frac{\Delta\rho_1^{(1)}}{\Delta\rho_2^{(2)}}\frac{C_2^e}{C_1^e} - 1\right) \tag{11}$$

When $\alpha = 1$ (i.e., for coarse-grained rocks that do not lose particles in the subsurface), Eqs. (7a), (7b)–(11) can be combined to yield:

$$\frac{Q_{gw}}{Q_p} = \frac{\Delta\rho_2^{(2)} C^e{}_1}{\Delta\rho_1^{(1)} C^e{}_2} \tag{12}$$

or, alternately,

$$E = W = \frac{q_p C^e{}_1}{\Delta\rho_1^{(1)}} = \frac{Q_{gw} C^e{}_2}{A_R \Delta\rho_2^{(2)}}. \tag{13}$$

These equations document that Q_{int}/Q_{gw} is constrained by the loss of the major porosity- and soil-initiating minerals and their solubilities. In the next sections we show that this treatment roughly describes the three case studies.

7.2. Linear hill model applied to VA granite

We first apply Eqs. ((10)–(13) to the VA granite (Bazilevskaya et al., 2013) using estimates of MAP – ET = $q_p = 0.38$ m y^{-1} and $A_R = 1.1$ km^2 for the Davis Run watershed in VA (Pavich et al., 1989). The volume change (strain) during weathering was taken into account (Brimhall and Dietrich, 1987) because strain influences the mineral concentrations when they are expressed per bulk volume of rock (see supplemental information).

The granite weathering profile initiates with oxidation of biotite (to form weathered rock) at RF_2, but this reaction also initiates the major increase in porosity associated with dissolution of plagioclase to form saprolite (Bazilevskaya et al., 2013). The major porosity-initiating reaction occurs at the weathered rock/saprolite interface. We therefore assumed that $\Delta\rho_2^{(2)} = 1.017$ kmol Na_2O m^{-3} (Table S2). Significant mass loss also occurs at RF_1, the soil-initiating reaction (at the saprolite/massive soil interface) because of dissolution of the potassium-containing minerals (potassium feldspar, muscovite, and biotite; Table S2). Therefore, $\Delta\rho_1^{(1)} = 0.435$ K_2O kmol m^{-3}. We assumed that Q_{int} flows at the massive soil/saprolite interface and that Q_{gw} flows at the saprolite/weathered rock interface.

Using Eq. (13) and $E = 6$ m My^{-1}, we calculate C_1^e ($=14.4$ mmol K m^{-3}). This value is not unreasonable in comparison to measured values of the maximum dissolved concentrations of potassium (58.8 mmol K m^{-3}) shown in Table S3 for a stream, Davis Run, sampled on the VA granite (Pavich, 1986). To estimate C_2^e, we use the average concentration of Na in Davis Run (Table S4, 261 mmol Na m^{-3}) which we assumed was a good estimator for groundwater as it is likely to reflect baseflow (Pavich, 1986). These values substituted into Eq. (11) yield $Q_{int}/Q_{gw} = 0.9$ (assuming no contribution from particulates, i.e., $\alpha = 1$). This rough estimate is not dissimilar to the value of 0.67 estimated by Pavich (1986). Furthermore, if significant road salt contributes Na to the stream as suggested by Pavich et al. (1985), the actual value of C_2^e would be lower and would yield a lower ratio of Q_{int}/Q_{gw}. Using $Q_p = 4.2 \times 10^5$ m^3 y^{-1} as reported for the Virginia site and $Q_{int}/Q_{gw} = 0.9$, we also estimate $Q_{gw}/A_R = 0.20$ m y^{-1} and $Q_{int}/A_R = 0.18$ m y^{-1}.

7.3. Linear hill model applied to VA diabase

We complete the same calculations using Eqs. (10)–(13) for the weathering diabase. Once again, we assume that the deepest reaction (dissolution of ferrous pyroxene) sets RF_2, but is coincident with onset of the major porosity-initiating reaction (dissolution of augite). In this case it is difficult to distinguish groundwater flow (moving at the weathered rock/saprolite interface) from interflow (moving at the saprolite/massive soil interface) because the plagioclase (RF_1) and pyroxene (RF_2) reaction fronts do not separate significantly (Fig. 2). After calculating and correcting for strain (supplemental information), the loss of Na_2O at the saprolite/soil interface (RF_1) was used to define loss of plagioclase, $\Delta\rho_1^{(1)} = 1686$ $Na_2O/2$ mol m^{-3}, while the loss of CaO at the weathered rock/saprolite interface (RF_2) was used to define loss of pyroxene, $\Delta\rho_2^{(2)} = 1097$ CaO mol m^{-3} (Table S5).

Following the approach described above for the VA granite and using Eq. (13) with the same values of E ($=6$ m My^{-1}) and q_p ($=0.38$ m $year^{-1}$), C_1^e was estimated to equal 0.027 mol Na m^{-3} (Eq. (13)). An estimate for C_2^e was derived from porewater Ca measured for the 0.1 to 2.1 m depth interval for a diabase weathering in Pennsylvania (Yesavage et al., 2016): ~0.23 mol Ca m^{-3} (Table S6). With this value of C_2^e, Eq. (11) yields $Q_{int}/Q_{gw} \approx 12.1$.

Although these concentrations are all poorly constrained, Q_{int}/Q_{gw} is a high value because of the nature of diabase: loss of the oxide component from the massive soil-initiating mineral is larger at RF_1 than loss of the oxide component from the major-porosity initiating mineral at RF_2 because $\frac{\Delta\rho_1^{(1)}}{\Delta\rho_2^{(2)}} > 1$. When this condition is met, it is likely from Eq. 11 that $Q_{int}/Q_{gw} > 1$ since $\frac{C_2^e}{C_1^e} > 1$ (the mineral dissolving at RF_1 is by definition less soluble than the mineral at RF_2.) At the most simple level, the condition $\frac{\Delta\rho_1^{(1)}}{\Delta\rho_2^{(2)}} > 1$ is likely for the diabase because the rock has more plagioclase (dissolves at RF_1) than pyroxene (dissolves at RF_2). In contrast, for the granite, $\frac{\Delta\rho_1^{(1)}}{\Delta\rho_2^{(2)}} < 1$ because this two-feldspar granite has more plagioclase (RF_2) than potassium feldspar (RF_1).

Also notable, although $\frac{C_2^e}{C_1^e} > 1$ for 2 = Na and 1 = K simply because the plagioclase feldspars have higher solubilities than the alkali feldspars, vegetation also affects the ratio $\frac{C_2^e}{C_1^e}$ by working to retain nutrients in the upper layers. This in turn is likely to increase the aqueous concentration of K compared to an abiotic analogue, affecting Q_{int}/Q_{gw}. In effect, vegetation retains and recycles K in the upper layers (Brantley et al., 2012), stabilizing K-containing minerals by increasing aqueous K concentrations. On the other hand, vegetation also returns water to the atmosphere through evapotranspiration, a process which decreases Q_{int} and Q_{gw}. Overall, vegetation is therefore likely to shunt less water to interflow (Brantley et al., 2012).

7.4. Linear hill model applied to Shale Hills

We also use Eq. (11) for Shale Hills where the major porosity-initiating mineral is assumed to be ankeritic calcite (dissolution initiates at RF_2) and the soil-initiating mineral is illite (RF_1). The ankerite and illite losses at RF_2 and RF_1 yield $\Delta\rho_2^{(2)} = 215$ and $\Delta\rho_1^{(1)} = 579$ kg m^{-3} of bedrock (Table S7). The shale is thus more similar to the diabase than the granite in that $\frac{\Delta\rho_1^{(1)}}{\Delta\rho_2^{(2)}} > 1$. In this case where we have ample field data, estimates for the solute concentrations were derived from groundwater measurements: $C_1^e = 0.0133$ g/L of illite and $C_2^e = 0.15$ g/L of $(Ca_{0\cdot8}Mg_{0.2})CO_3$. However, more than half of the total clay removed is removed in the subsurface as particulates (Sullivan et al., in press): we therefore set $\alpha = 2.5$. Inserting these values into Eq. (11) yields $Q_{int}/Q_{gw} = 12$. This value is very similar to Q_{int}/Q_{gw} estimated based on hydraulic conductivities by Sullivan et al. (in press): ~10.

In this case, because we did not use E to calculate C_1^e from Eq. (13), we instead use Eqs. (10) and (7a) and (7b) to calculate Q_{gw} and Q_{int}. We used the average erosion rate (assumed equal to the weathering advance rate, W) for Shale Hills of 30 m/My (West et al., 2014) and the watershed surface area (A_R) of 0.08 km^2. Eq. (10b) yields $Q_{gw} = 3 \times 10^3$ m^3 y^{-1}. This value agrees with published estimates estimated for groundwater outflow by other means at Shale Hills (3×10^3 m^3 y^{-1}) by Lin (2006).

8. Lithology and Q_{int}/Q_{gw}

These examples are order-of-magnitude estimates that were discussed to show that the linear hill mass balance is a useful representation for some systems. In fact, the ratio of Q_{int} to Q_{gw} might be possible to estimate even for poorly defined systems just on the basis of rock composition alone. This would address the need for better conceptual models for groundwater systems as articulated in the literature (Banks et al., 2009; MacQuarrie et al., 2010).

As an example, we calculate Q_{int}/Q_{gw} for another felsic system in the Piedmont where we have even less information: Pond Branch, a watershed developed on a metapelite (Cleaves et al., 1970). No concentration vs. depth data were reported; however, the initial metapelite has ~10.6% plagioclase, 23.9% muscovite, and 9.8% biotite (Cleaves et al., 1970). The main dissolution reactions are observed to be weathering of Na and Ca-containing plagioclase and K-containing mica (Cleaves et al., 1970; Pavich et al., 1989).

Applying the linear hill calculations (Eqs. ((10)–(13)) to Pond Branch, we choose Na and K as components 2 and 1 respectively. Dissolution of plagioclase (with composition of 22% anorthite) is assumed to initiate at RF_2 (component 2 = Na, $\Delta\rho_2^{(2)} \approx 825$ mol Na per m^3 of rock) and biotite at RF_1 (component 1 = K, $\Delta\rho_1^{(1)} \approx 670$ mol K per m^3). With the reported values of 1.9 ppm K (0.049 mol m^{-3}) in interflow and 1.5 ppm Na (0.065 mol m^{-3}) in baseflow (Cleaves et al., 1970), and $(MAP - ET) = 0.18$ m y^{-1} (Cleaves et al., 1970), we calculate $Q_{int}/A_R = 0.013$ m y^{-1}, $Q_{gw}/A_R = 0.167$ m y^{-1}, and $Q_{int}/Q_{gw} \approx 0.08$.

Assuming that water leaves the catchment either as baseflow or interflow, and equating baseflow to groundwater flow, this value of Q_{int}/Q_{gw} is consistent with loss of 92% of water that enters the catchment as groundwater. This value is in turn surprisingly consistent with the published estimate ($Q_{int}/Q_{gw} \approx 0.1$) that 90% of the water left the catchment as baseflow (Cleaves et al., 1970). Instead of relying on observations from stream chemistry, we could have calculated Q_{int}/Q_{gw} from estimated solubilities for albite (6×10^{-4} mol m^{-3}) and potassium feldspar (3×10^{-4} mol m^{-3}) in pure water (Berner, 1981). In this case the estimate is $Q_{int}/Q_{gw} \approx 0.7$, consistent again with most of the water (~60%) leaving as groundwater flow.

Thus even for systems without mineral depth profiles or stream chemistry observations, the approach has utility. Patterns of Q_{int}/Q_{gw} for steady state systems might therefore be predictable from lithology: from Eq. (11) we predict that Q_{int}/Q_{gw} should be largest for protoliths with a trace amount of a highly soluble mineral in a mostly insoluble and impermeable matrix, i.e., high values of C_2^e/C_1^e and $\Delta\rho_1^{(1)}/\Delta\rho_2^{(2)}$ respectively. This describes, for example, a low-permeability quartz-dominated sandstone with minor calcite and alkali feldspar. In this case, component 1 is potassium present in relatively insoluble alkali feldspar and 2 is $CaCO_3$ present in trace quantities as the soluble mineral calcite. Assuming solubilities in pure water of potassium feldspar and calcite of 3×10^{-4} and 0.06 mol m^{-3}, respectively (Berner, 1981), yields $Q_{int}/Q_{gw} >> 1$. In this case, Eq. (12) is consistent with 0.5% of the meteoric influx leaving as groundwater flow from a low-permeability sandstone that contains 5% calcite (major porosity-initiating mineral) and 5% potassium feldspar (soil-initiating mineral).

These ideas can also be applied to igneous rocks ranging from felsic to mafic compositions. This gradient varies from granites that contain abundant quartz, both types of feldspars (alkali feldspars with potassium and plagioclase feldspars with sodium/calcium), and micas; to diorites with plagioclase feldspar, minor quartz, mica, and amphibole; to diabase (gabbroic rocks) with mainly plagioclase and pyroxene. Regardless of the mineralogy, $C_1^e < C_2^e$ because mineral 2 dissolves at depth and mineral 1 dissolves near the surface. To estimate a first-order approximation using Eq. (11), we therefore only consider $\Delta\rho_1^{(1)}/\Delta\rho_2^{(2)}$. In a granite where $\Delta\rho_1^{(1)}/\Delta\rho_2^{(2)} < 1$ (1 refers to potassium minerals alkali feldspar + mica; 2 refers to plagioclase), the value of Q_{int}/Q_{gw} from Eq. (11) is <1 and most water leaves the hill as groundwater. In contrast, in a mafic rock (mineral 1 = plagioclase and 2 = pyroxene) such as the VA diabase discussed here, $\Delta\rho_1^{(1)}/\Delta\rho_2^{(2)} > 1$. Therefore, according to Eq. (11), more water leaves that rock as interflow than as groundwater.

With these calculations we are implying that groundwater will be greater than interflow at steady state in some hills simply because of the mineralogical composition. In effect, when a deep-reacting mineral is more abundant than a shallow-reacting mineral in a given lithology within a hill, a permeability structure will develop to allow more water to flow through the weathered rock as groundwater than through the upper layer as interflow. In this way, the more soluble and abundant mineral can be dissolved and removed at the same rate as the less soluble and less abundant mineral. Of course, such flow patterns cannot occur if the rock remains impermeable and unfractured, i.e., if it evolves like the VA diabase. For this reason, we have emphasized permeability-enhancing reactions. In fact, the compositional range that is likely to experience more groundwater than interflow overlaps with the composition that is likely to experience oxidation-induced fracturing because this composition often contains biotite. The content of biotite may be a good predictor of weathering-induced fracturing and deep groundwater flow through weathered rock because biotite has been commonly observed to swell during oxidation and has been inferred to create fractures. This is consistent, for example, with the observation that regolith is thicker on biotite-bearing pelitic schists than sericite-chlorite phyllites in the Piedmont (Pavich et al., 1989) or that little weathering occurs on biotite-lacking leucogranites but deep weathering occurs on biotite granites (Dewandel et al., 2006).

Of course, the ratio of O_2 to CO_2 in the soil atmosphere varies from location to location, and high O_2 in the soil atmosphere in some areas might allow oxidation-induced fracturing to drive deep infiltration even in rock with high FeO content. For example, in contrast to Fig. 2A, some diabase units in Virginia and Pennsylvania (PA) show spheroidal weathering (Pavich et al., 1989; Hausrath et al., 2011) and some have attributed this type of weathering to oxidation-induced fracturing (Fletcher et al., 2006). A difference between the VA diabase and the spheroidally weathered PA diabase is that the former is a slower-eroding, coarser-grained sill while the latter is a faster-eroding finer-grained dike. In the PA dike, for example, the grain size of the feldspar and pyroxene varies between hundreds of microns and 1 mm, whereas in the VA diabase the grain size is 1–2 mm. In the Piedmont, finer-grained diabase units exhibit better-developed jointing than the coarser-grained units (Roberts, 1928). Such jointing likely allows oxygenated water to access deeper parts of the diabase profile. Under such well-drained conditions, oxygen may be maintained at concentrations that crack the rock even though it is FeO-rich ($R^o = 0.04$). The importance of fracture spacing in determining the depth of weathering on diabase in the VA Piedmont was emphasized previously by Pavich et al. (1989).

In summary, in massive mafic rocks weathering in a hill at steady state, Q_{int}/Q_{gw} is large because the rock does not fracture during weathering and reaction fronts do not separate (Fig. 2). In felsic rocks that contain biotite, Q_{int}/Q_{gw} becomes small because the permeability increases because of weathering-induced fracturing driven by biotite oxidation deep in the profile. The ratio Q_{int}/Q_{gw} may also become small in pyrite-rich rocks that oxidize and develop deep high-flow zones. Given the importance of oxygen in driving fracturing, the actual delivery of oxygen to deep weathering—by preexisting vertical fractures in the system—also affects the extent of oxidation-induced fracturing.

9. Reaction front depth intervals as valves

If hills weather and erode at steady state, then these calculations show that the permeability of the interfaces between the soil, saprolite, and weathered rock must evolve until $\frac{Q_{gw}}{Q_p} = \frac{\Delta\rho_2^{(2)}}{\Delta\rho_1^{(1)}}\frac{C^e{}_1}{C^e{}_2}$ (Eq. 12). In other words, hills that contain minerals of different solubility and reactivity evolve to develop permeability in the upper flow zone, K_{int}, and lower flow zone, K_{gw}, that allows the partitioning of Q_p into Q_{int} and Q_{gw} so that $U = E = W$. This idea is an extension to the idea promoted earlier by Pavich (1986): soil acts 'to partition rainfall into evapotranspiration, runoff, and recharge to the saprolite'. We argue that the hill itself develops a permeability architecture consisting of massive soil and soil, characterized by slow-dissolving mineral reactions (often the alkali-containing minerals), and saprolite and weathered rock, characterized by fast-dissolving mineral reactions (often, Na- and Ca-containing minerals) and that this architecture partitions Q_p into Q_{int} and Q_{gw} (see Fig. 7):

$$\frac{Q_{\text{int}}}{Q_{gw}} = \frac{H_{\text{int}}}{H_{gw}}\frac{K_{\text{int}}}{K_{gw}}\frac{\Delta B_1}{\Delta B_2} \tag{14}$$

Certain depth intervals act as valves that partition the water flows, and the reaction fronts at these depths can cause the valve behavior and record the water flows at the valves.

As pointed out previously, the ratio $\frac{\Delta\rho_1^{(1)}}{\Delta\rho_2^{(2)}}$ largely determines whether Q_{int} and Q_{gw} are both important at steady state. In the granite, the ratio (i.e., the ratio of potassium to plagioclase feldspar) is <1, and most water leaves the hill as groundwater. In contrast, in the Rose Hill shale, the ratio > 1, and most water leaves as interflow. The zones of high-volume flow in these two quartzo-feldspathic rocks are separated over tens of meters depth. Like the shale, the value of $\frac{\Delta\rho_1^{(1)}}{\Delta\rho_2^{(2)}}$ for the diabase, i.e., the ratio of plagioclase feldspar to pyroxene, is >1, and most water leaves as interflow. However, in the massive diabase, the feldspar and pyroxene reaction fronts are closely co-located, and interflow and groundwater flow are co-located within a narrow depth interval. In the more felsic shale and granite, RF_1 and RF_2 separate by meters.

The separation of reaction fronts is determined partly by chemistry (soil gas, mineral composition, mineral abundance) and partly by the density of fractures. Felsic or highly fractured rocks separate into upper and lower dissolution zones that host interflow and groundwater flow respectively. The upper zone is dominated by dissolution by CO_2 and organic acids while the lower zone is dominated by reactions with O_2, the remaining CO_2, and any H_2SO_4 generated by pyrite. In contrast, massive mafic rocks with low R^o are not as likely to develop separated fronts because they are less likely to experience oxidation-induced fracturing. Unless they are characterized by preexisting fractures due to cooling or tectonics, these lithologies develop only one zone of important lateral flow because the reaction fronts remain narrow and unseparated with little of the water flow penetrating weathering rock. Even when these rocks are fractured, regolith depth, and separation of fronts remains smaller than on quartzo-feldspathic rocks (Pavich et al., 1989).

When the permeability of the interflow zone is much larger than that of the groundwater flow zone and $\Delta B_1 \geq \Delta B_2$, as observed for rocks like the Rose Hill shale, much of the solubilized mass of the rock leaves the system in interflow. In contrast, when $\frac{\Delta\rho_1^{(1)}}{\Delta\rho_2^{(2)}} < 1$, much of the solubilized mass leaves at depth because of the high secondary permeability in the weathered rock. For example, in massive granites in the Piedmont that have very little primary permeability, drillers report highly permeable sand and boulders at the saprolite-weathered rock interface (Nutter, 1969). We argue that this high permeability results from weathering-induced fracturing and oxidative dissolution (of pyrite and biotite especially) and we point to previous studies as evidence for such phenomena (Jones, 1985; Taylor and Eggleton, 2001; Dewandel et al., 2006; Legout et al., 2007; Ayraud et al., 2008; Buss et al., 2008; Lachassagne et al., 2011; Brantley et al., 2013b; Navarre-Sitchler et al., 2015).

Finally, it is important to note that the notion of steady state for weathering and erosion is perhaps a ‘convenient fiction’ (Phillips, 2010). Steady state is nonetheless often assumed and is probably useful in temperate regions such as the Piedmont rocks discussed throughout this paper (Pavich et al., 1989). Our model may therefore be useful to understand such systems. On the other hand, the implications of our model—that mineral solubility must be taken into account in considerations of weathering advance and erosion rates if steady state is ever to be attained—may also be useful in assessing if steady state is operative in some systems.

10. Conclusions

Many observations of hills have documented that water can flow laterally in the mostly unsaturated zone as well as at depth (Tromp-van Meerveld et al., 2007; Ayraud et al., 2008; Katsura et al., 2008; van Meerveld et al., 2015). Conceptual and numerical models of such flow are needed.

We describe a conceptual model for hills on relatively impermeable bedrock in regions where precipitation is greater than potential evapotranspiration. In our model, water flows in two main zones of water table fluctuation: an upper *interflow zone* that forms when the water table is high or perched, and a lower *groundwater zone*. This latter zone may represent the zone of fluctuation of the regional water table but it can also be a layer well below the regional water table that is a zone of intense fracturing and friable weathered rock. Such deep fractured and friable layers have been identified repeatedly in groundwater studies of crystalline rock (e.g. Jones, 1985; Dewandel et al., 2006; Legout et al., 2007; Lachassagne et al., 2011). Importantly, the two zones of water table fluctuation are also depth intervals that record significant biogeochemical reaction, i.e., reaction fronts. Indeed, these reaction fronts may be a main cause of the porosity and permeability that maintain flow in the two zones. For example, clay precipitation or deposition may cause or contribute to the formation and maintenance of impermeable layers that underlie the upper flow zone. Likewise, the deep fractured and friable layer has been attributed to weathering-induced fracturing in crystalline rock at the base of the weathering profile (Buss et al., 2008; Lachassagne et al., 2011). Our model is very different from a recent model that emphasized only the properties of the protolith (Rempe and Dietrich, 2014) because our concept emphasizes the dual importance of the protolith and the regolith in controlling the fluxes of fluids and the depth of weathering.

The zone of interflow is typically co-located with a shallow reaction front (RF_1) near the bottom of soil or massive soil. The RF_1 is dominated especially by CO_2 and organic acid reactions and is often associated with formation of a clay layer that can act as an aquitard. A second important reaction front, RF_2, is co-aligned with or lies below the deeper regional groundwater table. The deepest reaction is typified by reactions with O_2 (especially felsic rocks), CO_2 (especially mafic rocks), or H_2SO_4 (pyrite-containing rocks). This deep reaction, RF_2, typically also delineates the onset of the major porosity-initiating reaction. In massive mafic rocks the two lateral flow zones do not tend to separate significantly, but in felsic rocks the zones can separate over tens of meters.

The reaction fronts document chemical loss or gain of minerals and are thus often characterized by contrasts in permeability. As such, the reaction front depth intervals act like valves that reorient unsaturated water flow from predominantly vertical to lateral. The shunting of vertical to lateral flow at RF_1 affects the rate of shallow and deep reactions because it removes reaction products from RF_1 at the same time that it controls the extent of infiltration of water and reactants to RF_2. Lateral flow at RF_2 removes the most soluble minerals as groundwater flow.

At the same time that downward flowing water is reoriented from vertical to lateral at reaction fronts, rock material that advects upward through eroding hills is similarly redirected from vertical to lateral flow. Specifically, the most soluble minerals first leave the system at RF_2 by dissolving into groundwater and flowing laterally to the channel. In felsic rocks this deep reaction zone typically marks the zone of consumption of O_2 and is then immediately followed by growth of porosity due to dissolution of plagioclase feldspar. Oxidative dissolution is accelerated in the zone of water table fluctuation in response to the entrainment of O_2 into groundwater as the water table moves up and down. If minerals are not dissolved at RF_2 or if the rate of upward advection of material is fast enough, unreacted minerals move up and through the dominantly unsaturated zone, and moderately soluble minerals reach RF_1 where they dissolve. Only the least soluble minerals are exposed and removed at the land surface by erosion. Whether a given mineral becomes exposed at the land surface is a function of the residence time in the hill (determined by the erosion rate), the lithology (how much mineral is initially present), and the volume of water that flows past the mineral while in the subsurface (determined by the infiltration rate).

During the transit of water and particles through the hill, feedbacks between porefluid chemistry, particle size, fracture density, and soil gas drive the hill toward the condition where rates of uplift = erosion = weathering advance. Biota are often involved in these feedbacks. The slope of the hill is set by the erosion rate while the slopes of the reaction fronts are set by the rates of water influx. Importantly, the slope of the RF_1 zone is controlled by precipitation (P) minus evapotranspiration (ET), but the slope of RF_2 is controlled by $P - ET$ - interflow.

The two reaction zones tend to separate by meters under hills on felsic rocks but centimeters on mafic rocks because permeability opens up during weathering of felsic rock because of weathering-induced fracturing that allows advection of water through reaction fronts. This infiltration increases the regolith thickness, reaction front thickness, and spacing of fronts. On massive mafic rocks, regolith and reaction fronts remain thinner, and chemical losses occur in co-located shallow lateral flows. The most important exception to this felsic vs. mafic contrast is when high fracture or joint densities created by tectonics or cooling or other pre-existing conditions allow significant infiltration of oxygenated fluids into mafic rock. In such cases, the drainage can promote spheroidal weathering, thicker regolith, and the separation of reaction fronts.

According to these ideas, hills evolve toward a permeability architecture that allows material to be removed from the hill at steady state as solutes and as particles. The permeability is an emergent property of the hill that allows partitioning of water to remove minerals of different solubilities and rock material of different fracture toughness. Such lithological considerations should be useful in generating the conceptual underpinnings of quantitative hillslope hydrology models. Further collection of data about hill architecture would aid in the development of numerical models that explore the feedbacks and evolution of fracture densities and chemical reactions and thus illuminate how hills work.

Acknowledgements

S. Brantley acknowledges NSF Critical Zone Observatory grants EAR 12-39285 and 13-31726 for support for working on the Susquehanna Shale Hills Critical Zone Observatory in Penn State's Stone Valley Forest. The Forest is supported and managed by the Penn State Forestland Management Office in the College of Agricultural Sciences. SLB, ML, and GS acknowledge funding from DOE OBES DE-FG02-OSER15675. SLB acknowledges discussions with F. Reis, S. Hynek, R. DiBiase, K. Bazilevskaya, C. Riebe, S. Holbrook, H. Kim, and D. Rempe, as well as other colleagues, and feedback from two anonymous reviewers.

Appendix A. Supplementary data

Supplementary data to this article can be found online at http://dx.doi.org/10.1016/j.geomorph.2016.09.027.

References

Amundson, R., 2004. Soil formation. In: Drever, J.I. (Ed.), Treatise in Geochemistry: Surface and Ground Water, Weathering, and Soils. Elsevier Pergamon, Amsterdam, pp. 1–35.

Anderson, S.P., Dietrich, W.E., Brimhall, G.H., 2002. Weathering profiles, mass balance analysis, and rates of solute loss: linkages between weathering and erosion in a small, steep catchment. Geol. Soc. Am. Bull. 114 (9), 1143–1158.

Ayraud, V., Aquilina, L., Labasque, T., Pauwels, H., Molenat, J., Pierson-Wickmann, A.-C., Durand, V., Bour, O., Tarits, C., Le Corre, P., Fourre, E., Merot, P., Davy, P., 2008. Compartmentalization of physical and chemical properties in hard-rock aquifers deduced from chemical and groundwater age analyses. Appl. Geochem. 23, 2686–2707. http://dx.doi.org/10.2610.1016/j.apgeochem.2008.2606.2001.

Bacon, A.R., Richter, D., Bierman, P.R., Rood, D.H., 2012. Coupling meteoric ^{10}Be with pedogenic losses of ^{9}Be to improve soil residence time estimates on an ancient North American interfluve. Geology 40, 847–850.

Balashov, V.N., Yardley, B.W.D., Lebedeva, M.I., 1999. Metamorphism in marbles: role feedbacks between reaction, fluid flow, pore pressure and creep. In: Jamtveit, B., Meakin, P. (Eds.), Growth, Dissolution and Pattern Formation in Geosystems. Kluwer Academic Publishers, Dordrecht, pp. 367–380.

Banks, E.W., Simmons, C.T., Love, A.J., Cranswick, R., Werner, A.D., Bestland, E.A., Wood, M., Wilson, T., 2009. Fractured bedrock and saprolite hydrogeologic controls on groundwater/surface-water interaction: a conceptual model (Australia). Hydrogeol. J. 17 (8), 1969–1989.

Bazilevskaya, E., Lebedeva, M., Pavich, M., Rother, G., Parkinson, D.Y., Cole, D., Brantley, S.L., 2013. Where fast weathering creates thin regolith and slow weathering creates thick regolith. Earth Surf. Proc. Land. 38 (8), 847–858. http://dx.doi.org/10.810.1002/esp.3369.

Bazilevskaya, E., Rother, G., Mildner, D.F.R., Pavich, M., Cole, D., Bhatt, M.P., Jin, L., Steefel, C.I., Brantley, S.L., 2014. How oxidation and dissolution in diabase and granite control porosity during weathering. Soil Sci. Soc. Am. J. http://dx.doi.org/10.2136/sssaj2014.2104.0135.

Behrens, R., Bouchez, J., Schuessler, J.A., Dultz, S., Hewawasam, T., von Blanckenburg, F., 2015. Mineralogical transformations set slow weathering rates in loc-porosity metamorphic bedrock on mountain slopes in a tropical climate. Chem. Geol. 411, 283–298. http://dx.doi.org/10.1016/j.chemgeo.2015.07.008.

Berner, R.A., 1981. Kinetics of weathering and diagenesis. In: Lasaga, A.C., Berner, R.A., Fisher, G.W., Anderson, D.E., Kirkpatrick, R.J. (Eds.), Kinetics of Geochemical Processes. Mineralogical Society of America, Washington D.C., pp. 111–134.

Bornstein, J., Hedstrom, W.E., Scott, F.R., 1980. Oxygen diffusion rate relationships under 3 soil conditions. Maine Agricultural Experiment Station: Orono Maine (U.S.A.), pp. 1–12.

Brantley, S.L., Lebedeva, M., 2011. Learning to read the chemistry of regolith to understand the critical zone. Annu. Rev. Earth Pl. Sci. 39, 387–416.

Brantley, S.L., White, A.F., 2009. Approaches to modeling weathered regolith. In: Oelkers, E., Schott, J. (Eds.), Thermodynamics and Kinetics of Water-rock Interaction. Rev. Mineral. Geochem., pp. 435–484.

Brantley, S.L., Buss, H., Lebedeva, M., Fletcher, R.C., Ma, L., 2011. Investigating the complex interface where bedrock transforms to regolith. Appl. Geochem. S12–S15 http://dx.doi.org/10.1016/j.apgeochem.2011.1003.1017.

Brantley, S.L., Lebedeva, M., Hausrath, E.M., 2012. A geobiological view of weathering and erosion. In: Knoll, A., Canfield, D., Konhauser, K. (Eds.), Fundamentals of Geobiology. Wiley-Blackwell, pp. 205–227 http://dx.doi.org/10.1002/9781118280874.

Brantley, S.L., Holleran, M.E., Jin, L., Bazilevskaya, E., 2013a. Probing deep weathering in the Shale Hills Critical Zone Observatory, Pennsylvania (U.S.A.): the hypothesis of nested chemical reaction fronts in the subsurface. Earth Surf. Proc. Land. http://dx.doi.org/10.1002/esp.3415.

Brantley, S.L., Lebedeva, M., Bazilevskaya, E., 2013b. Relating weathering fronts for acid neutralization and oxidation to pCO_2 and pO_2. In: Farquhar, J., Kasting, J., Canfield, D. (Eds.), Treatise of Geochemistry, the Atmosphere—History. Treatise on Geochemistry. Elsevier Amsterdam, The Netherlands.

Brimhall, G., Dietrich, W.E., 1987. Constitutive mass balance relations between chemical composition, volume, density, porosity, and strain in metasomatic hydrochemical systems: results on weathering and pedogenisis. Geochim. Cosmochim. Acta 51, 567–587.

Buol, S.W., Weed, S.B., 1991. Saprolite-soil transformations in the Piedmont and mountains of North Carolina. Geoderma 51, 15–28.

Burke, B.C., Heimsath, A.M., Dixon, J.L., Chappell, J., Yoo, K., 2009. Weathering the escarpment: chemical and physical rates and processes, south-eastern Australia. Earth Surf. Process. Landf. 1–18. http://dx.doi.org/10.1002/esp.1764.

Buss, H.L., Sak, P., Webb, R.M., Brantley, S., 2008. Weathering of the Rio Blanco quartz diorite, Luquillo Mountains, Puerto Rico: coupling oxidation, dissolution and fracturing. Geochim. Cosmochim. Acta 72, 4488–4507.

Calmels, D., Gaillardet, J., France-Lanord, C., Brenot, A., 2007. Sustained sulfide oxidation by physical erosion processes in the Mackenzie River basin: climatic perspectives. Geology 35, 1003–1006.

Carson, M.A., Kirkby, M.J., 1972. Hillslope Form and Process. Cambridge University Press, Cambridge.

Chigira, M., 1990. A mechanism of chemical weathering of mudstone in a mountainous area. Eng. Geol. 29, 119–138.

Chigira, M., Oyama, T., 1999. Mechanism and effect of chemical weathering of sedimentary rocks. Eng. Geol. 55, 3–14.

Chigira, M., Sone, K., 1991. Chemical weathering mechanisms and their effects on engineering properties of soft sandstone and conglomerate cemented by zeolite in a mountainous area. Eng. Geol. 30, 195–219.

Cleaves, E.T., 1993. Climatic impact on isovolumetric weathering of a coarse-grained schist in the northern Piedmont Province of the Central Atlantic states. Geomophology 8, 191–198.

Cleaves, E.T., Godfrey, A.E., Bricker, O.P., 1970. Geochemical balance of a small watershed and its geomorphic implications. Geol. Soc. Am. 81, 3015–3032.

Dewandel, B., Lachassagne, P., Wyns, R., Marechal, J.C., Krishnamurthy, N.S., 2006. A generalized 3-D geological and hydrogeological conceptual model of granite aquifers controlled by single or multiphase weathering. J. Hydrol. 330, 260–284. http://dx.doi.org/10.210.1016/j.jhydrol.2006.1003.1026.

Drake Jr., A.A., Froelich, A.J., 1977. Bedrock Map of Fairfax County, Va., U.S. Geological Open-file Report 77-523, Scale 1:48,000. United States Geological Survey.

Drake, H., Tullborg, E., MacKenzie, A.B., 2009. Detecting the near-surface redox front in crystalline bedrock using fracture mineral distribution, geochemistry and U-series disequilibrium. Appl. Geochem. 24, 1023–1039.

Duffy, C., Shi, Y., Davis, K., Slingerland, R., Li, L., Sullivan, P.L., Godderis, Y., Brantley, S.L., 2014. Designing a suite of models to explore critical zone function. Proc. Earth Planet. Sci. 7–15. http://dx.doi.org/10.1016/j.proeps.2014.1008.1003.

Eggler, D.H., Larson, E.E., Bradley, W.C., 1969. Granites, grusses, and the Sherman erosion surface, southern Laramie range, Colorado-Wyoming. Am. J. Sci. 267, 510–522.

Feakes, C.R., Holland, H.D., Zbinden, E.A., 1989. Ordovician Paleosols at Arisaig, Nova Scotia, and the evolution of the atmosphere. In: Bronger, A., Catt, J.A. (Eds.), Paleopedology: Nature and Application of Paleosols. Catena Supplement 16, pp. 207–232.

Fetter, C.W., 2001. Applied Hydrogeology. Prentice Hall, Upper Saddle River, New Jersey (U.S.A.).

Fletcher, R.C., Brantley, S.L., 2010. Reduction of bedrock blocks as corestones in the weathering profile: observations and model. Am. J. Sci. 310, 131–164. http://dx.doi.org/10.110.2475/2403.2010.2401.

Fletcher, R.C., Buss, H.L., Brantley, S.L., 2006. A spheroidal weathering model coupling porewater chemistry to soil thicknesses during steady-state denudation. Earth Planet. Sc. Lett. 244 (1–2), 444–457.

Follain, S., Minasny, B., McBratney, A.B., Walter, C., 2006. Simulation of soil thickness evolution in a complex agricultural landscape at fine spatial and temporal scales. Geoderma 133, 71–86.

Gleeson, T., Befus, K.M., Jasechko, S., Luijendijk, E., Bayani Cardenas, M., 2015. The global volume and distribution of modern groundwater. Nat. Geosci. http://dx.doi.org/10.1038/NGEO2590.

Godderis, Y., Francois, L., Probst, A., Schott, J., Moncoulon, D., Labat, D., Viville, D., 2006. Modelling weathering processes at the catchment scale: the WITCH numerical model. Geochim. Cosmochim. Acta 70, 1128–1147.

Graham, C.B., Woods, R.A., McDonnell, J.J., 2010. Hillslope threshold response to rainfall: (1) a field based forensic approach. J. Hydrol. 393 (1–2), 65–76.

Hack, J.T., 1960. Interpretation of erosional topography in humid temperate regions. Am. J. Sci. 258, 80–97.

Hausrath, E., Navarre-Sitchler, A.K., Sak, P.B., Williams, J.Z., Brantley, S.L., 2011. Soil profiles as indicators of mineral weathering rates and organic interactions on a Pennsylvania diabase. Chem. Geol. 290 (3–4), 89–100.

Hilley, G.E., Chamberlain, C.P., Moon, S., Porder, S., Willett, S.D., 2010. Competition between erosion and reaction kinetics in controlling silicate-weathering rates. Earth Planet. Sc. Lett. 293, 191–199. http://dx.doi.org/10.110.1016/j.epsl.2010.1001.1008.

Holbrook, W.S., Riebe, C.S., Elwaseif, M., Hayes, J.L., Basler-Reeder, K., Harry, D.L., Malazian, A., Dosseto, A., Hartsough, P.C., Hopmans, J.W., 2014. Geophysical constraints on deep weathering and water storage potential in the Southern Sierra Critical Zone Observatory. Earth Surf. Proc. Land. 39, 366–380. http://dx.doi.org/10.310.1002/esp.3502.

Holland, H.D., Zbinden, E.A., 1988. Paleosols and the evolution of the atmosphere: part I. In: Lerman, A., Meybeck, M. (Eds.), Physical and Chemical Weathering in Geochemical Cycles. Kluwer Academic Publishers, New York.

Hooper, R.P., Christophersen, N., Peters, N.E., 1990. Modelling stream-water chemistry as a mixture of soilwater end-members: an application to the Panola Mountain catchment, Georgia, USA. J. Hydrol. 116, 32–43.

Hopp, L., McDonnell, J.J., 2009. Connectivity at the hillslope scale: identifying interactions between storm size, bedrock permeability, slope angle and soil depth. J. Hydrol. 376, 378–391.

Jamtveit, B., Hammer, O., 2012. Sculpting of rocks by reactive fluids. Geochem. Perspect. 1, 341–480.

Jin, L., Ravella, R., Ketchum, B., Bierman, P.R., Heaney, P., White, T., Brantley, S.L., 2010. Mineral weathering and elemental transport during hillslope evolution at the Susquehanna/Shale Hills Critical Zone Observatory. Geochim. Cosmochim. Acta 74 (13), 3669–3691.

Jin, L., Rother, G., Cole, D.R., Mildner, D.F.R., Duffy, C.J., Brantley, S.L., 2011. Characterization of deep weathering and nanoporosity development in shale – a neutron study. Am. Mineral. 96, 498–512. http://dx.doi.org/10.410.2138/am.2011.3598.

Jobbagy, E.G., Jackson, R.B., 2001. The distribution of soil nutrients and depth: global patterns and the imprint of plants. Biogeochemistry 53, 51–77.

Jones, M.J., 1985. The weathered zone aquifers of the basement complex areas of Africa. Q. J. Eng. Geol. London 18, 35–46.

Katsura, S., Kosugi, K., Mizutani, T., Okunaka, S., Mizuyama, T., 2008. Effects of bedrock groundwater on spatial and temporal variations in soil mantle groundwater in a steep granitic headwater catchment. Water Resour. Res. 44. http://dx.doi.org/10.1029/2007WR00610.

Lachassagne, P., Wyns, R., Dewandel, B., 2011. The fracture permeability of Hard Rock Aquifers is due neither to tectonics, nor to unloading, but to weathering processes. Terra Nova 23 (3), 145–161.

Lebedeva, M., Brantley, S.L., 2013. Exploring geochemical controls on weathering and erosion of convex hillslopes: beyond the empirical regolith production function. Earth Surf. Proc. Land. 38 (15), 1793–1807. http://dx.doi.org/10.1002/esp.3424.

Lebedeva, M.I., Fletcher, R.C., Balashov, V.N., Brantley, S.L., 2007. A reactive diffusion model describing transformation of bedrock to saprolite. Chem. Geol. 244 (3–4), 624–645.

Lebedeva, M.I., Fletcher, R.C., Brantley, S.L., 2010. A mathematical model for steady-state regolith production at constant erosion rate. Earth Surf. Process. Landf. 35 (5), 508–524.

Legout, C., Molenat, J., Aquilina, L., Gascuel-Odoux, C., Faucheux, M., Fauvel, Y., Bariac, T., 2007. Solute transfer in the unsaturated zone-groundwater continuum of a headwater catchment. J. Hydrol. 332, 427–441. http://dx.doi.org/10.1016/j.jhydrol.2006.07.017.

Lichtner, P.C., 1988. The quasi-stationary state approximation to coupled mass transport and fluid-rock interaction in a porous medium. Geochim. Cosmochim. Acta 52, 143–165.

Lichtner, P.C., Waber, N., 1992. Redox front geochemistry and weathering: theory with application to the Osamu Utsumi uranium mine, Pocos de Caldas, Brazil. J. Geochem. Explor. 45, 521–564.

Lin, H.S., 2006. Temporal stability of soil moisture spatial pattern and subsurface preferential flow pathways in the Shale Hills Catchment. Vadose Zone J. 5, 317–340.

Lonsdale, J.T., 1927. Geology of the gold-pyrite belt of the northeastern Piedmont, Virginia. Va. Geol. Surv. Bull. 30, 1–110.

MacQuarrie, K.T.B., Mayer, K.U., Jin, B., Spiessl, S.M., 2010. The importance of conceptual models in the reactive transport simulation of oxygen ingress in sparsely fractured crystalline rock. J. Contam. Hydrol. 112 (1–4), 64–76.

Maher, K., 2011. The role of fluid residence time and topographic scales in determining chemical fluxes from landscapes. Earth Plan. Sci. Lett. 312, 48–58. http://dx.doi.org/10.1016/j.epsl.2011.09.040.

McDonnell, J.J., 1990. A rationale for old water discharge through macropores in a steep, humid catchment. Water Resour. Res. 26 (11), 2821–2832.

McGlynn, B.L., McDonnell, J.J., 2003. Role of discrete landscape units in controlling catchment dissolved organic carbon dynamics. Water Resour. Res. 39 (4). http://dx.doi.org/10.1029/2002WR001525.

McGuire, K.J., McDonnell, J.J., 2010. Hydrological connectivity of hillslopes and streams: Characteristic time scales and nonlinearities. Water Resour. Res. 46, W10543. http://dx.doi.org/10.10510.11029/12010WR009341.

Minasny, B., McBratney, A.B., Salvador-Blanes, S., 2008. Quantitative models for pedogenesis - a review. Geoderma 144, 140–157.

Molnar, P., Anderson, R.S., Anderson, S.P., 2007. Tectonics, fracturing of rock, and erosion. J. Geophys. Res. 112, 1–12, F03014. http://dx.doi.org/10.11029/12005JF000433.002007.

Moore, J., Lichtner, P.C., White, A.F., Brantley, S.L., 2012. Using a reactive transport model to elucidate differences between laboratory and field dissolution rates in regolith. Geochim. Cosmochim. Acta 93, 235–261.

Mudd, S.M., Furbish, D.J., 2004. Influence of chemical denudation on hillslope morphology. J. Geophys. Res. - Earth 109, F02001.

Nadan, B.J., Engelder, T., 2009. Microcracks in New England granitoids: a record of thermoelastic relaxation during exhumation of intracontinental crust. Geol. Soc. Am. Bull. 121 (1–2), 80–99. http://dx.doi.org/10.1130/B26202.26201.

Navarre-Sitchler, A., Brantley, S.L., 2007. Basalt weathering across scales. Earth Planet. Sci. Lett. 261 (1–2), 321–334.

Navarre-Sitchler, A., Cole, D.R., Rother, G., Jin, L., Buss, H.L., Brantley, S.L., 2013. Porosity and surface area evolution during weathering of two igneous rocks. Geochim. Cosmochim. Acta 109, 400–413. http://dx.doi.org/10.410.1016/j.gca.2013.1002.1012.

Navarre-Sitchler, A., Brantley, S.L., Rother, G., 2015. How porosity increases during incipient weathering of crystalline silicate rocks. In: Steefel, C., Emmanuel, S., Anovitz, L. (Eds.), Pore-scale Geochemical ProcessesSoc. Am. - Geo. Soc.MIneral, pp. 331–354.

Nesbitt, H.W., Markovics, G., 1997. Weathering of a granodioritic crust, long-term storage of elements in weathering profiles, and petrogenesis of siliciclastic sediments. Geochim. Cosmochim. Acta 61 (8), 1653–1670.

Nordstrom, D.K., 2000. Advances in the hydrogeochemistry and microbiology of acid mine waters. Int. Geol. Rev. 42 (6), 499–515.

Nutter, L., 1969. Ground-water occurrence in the Maryland Piedmont. Maryland Geological Survey Report of Investigations 10, 1–54.

Ollier, C.D., 1967. Spheroidal weathering, exfoliation and constant volume alteration. Zeitschrift fuer Geomorphologie 11 (1), 103–108.

Pain, C.F., Ollier, C.D., 1996. Regolith stratigraphy: principles and problems. J. Aust. Geol. 16 (3), 197–202.

Pavich, M.J., 1986. Processes and rates of saprolite production and erosion on a foliated granitic rock of the Virginia Piedmont. In: Colman, S.M., Dethier, D.P. (Eds.), Rates of Chemical Weathering of Rocks and Minerals. Academic Press, Orlando, FL, pp. 551–590.

Pavich, M.J., Brown, L., Valette-Silver, J.N., Klein, J., Middleton, R., 1985. ^{10}Be analysis of a quaternary weathering profile in the Virginia Piedmont. Geology 13 (1), 39–41.

Pavich, M., Leo, G.W., Obermeier, S.F., Estabrook, J.R., 1989. Investigations of the characteristics, origin, and residence time of the upland residual mantle of the Piedmont of Fairfax County, Virginia. U. S. Geol. Surv. Prof. Pap. 1352, 1–58 U.S. Geological Survey.

Pelletier, J.D., 2008. Quantitative Modeling of Earth Surface Processes. Cambridge Univ, Press.

Peters, N.E., Freer, J., Aulenbach, B.T., 2003. Hydrologic dynamics of the Panola Mountain Research Watershed, Georgia. Ground Water 41, 973–988.

Phillips, J.D., 2010. The convenient fiction of steady-state soil thickness. Geoderma 156, 389–398. http://dx.doi.org/10.310.1016/j.geoderma.2010.1003.1008.

Portenga, E.W., Bierman, P.R., 2011. Understanding Earth's eroding surface with ^{10}Be. GSA Today 21, 4–10.

Price, J.R., Heitmann, N., Hull, J., Szymanski, D., 2008. Long-term average mineral weathering rates from watershed geochemical mass balance methods: using mineral modal abundances to solve more equations in more unknowns. Chem. Geol. 254, 36–51.

Rasmussen, C., Troch, P.A., Chorover, J., Brooks, P., Pelletier, J., Huxman, T.E., 2011. An open system framework for integrating critical zone structure and function. Biogeochemistry 102, 15–29.

Rempe, D.M., Dietrich, W.E., 2014. A bottom-up control on fresh-bedrock topography under landscapes. Proc. Natl. Acad. Sci. U. S. A. 111 (18), 6576–6581.

Rice Jr., T.J., Buol, S.W., Weed, S.B., 1985. Soil saprolite profiles, derived from mafic rocks in the North Carolina Piedmont. I. Chemical, morphological, and mineralogical characteristics and transformations. Soil Sci. Soc. Am. J. 49, 171–178.

Riebe, C.S., Kirchner, J.W., Granger, D.E., Finkel, R.C., 2001. Strong tectonic and weak climatic control of long-term chemical weathering rates. Geology 29 (6), 511–514.

Roberts, J.K., 1928. The geology of the Triassic. State of Virginia, conservation and development commission. Va Geol. Surv. Bull. 29, 1–177.

Salve, R., Rempe, D.M., Dietrich, W.E., 2012. Rain, rock moisture dynamics, and the rapid response of perched groundwater in weathered, fractured argillite underlying a steep hillslope. Water Resour. Res. 48, 25.

Shuman, B.N., Marsicek, J., 2016. The structure of Holocene climate change in mid-latitude North America. Quat. Sci. Rev. 141, 38–51. http://dx.doi.org/10.1016/j.quascirev.2016.03.009.

Smith, R.C., Rose, A.W., Lanning, R.M., 1975. Geology and geochemistry of Triassic diabase in Pennsylvania. Geol. Soc. Am. Bull. 86, 943–955.

St. Clair, J., Moon, S., Holbrook, S., Perron, J.T., Riebe, C.S., Martel, S., Carr, B., Harman, C., Singha, K., Richter, D., 2015. Geophysical imaging reveals topographic stress control of bedrock weathering. Science 350 (6260), 534–538. http://dx.doi.org/10.510.1126/science.aab2210.

Stallard, R., 1995. Relating chemical and physical erosion. In: White, A.F., Brantley, S.L. (Eds.), Chemical Weathering Rates of Silicate Minerals. Reviews in Mineralogy. Mineralogical Society of America, Washington, D.C., pp. 543–564.

Stallard, R.F., Edmond, J.M., 1983. Geochemistry of the Amazon 2. The influence of geology and weathering environment on the dissolved load. J. Geophys. Res. 88, 9671–9688.

Steefel, C.I., 1993. 1DREACT: User Manual and Programmer's Guide. Richland, WA.

Sullivan, P.L., Hynek, S., Gu, X., Singha, K., White, T.S., West, N., Kim, H., Clarke, B., Kirby, E., Duffy, C., Brantley, S.L., 2016. Oxidative dissolution under the channel leads geomorphological evolution at the Shale Hills catchment. Am. J. Sci. (in press).

Tague, C., Grant, G.E., 2004. A geological framework for interpreting the low-flow regimes of Cascade streams, Willamette River basin, Oregon. Water Resour. Res. 40 (W04303). http://dx.doi.org/10.1029/2003WR002629.

Taylor, G., Eggleton, R.A., 2001. Regolith Geology and Geomorphology. John Wiley and Sons, Chichester.

Torres, M.A., West, A.J., Li, G., 2014. Sulphide oxidation and carbonate dissolution as a source of CO_2 over geological timescales. Nature 507, 346–349. http://dx.doi.org/10.310.1038/nature13030.

Tóth, J., 1970. A conceptual model of the groundwater regime and the hydrogeologic environment. J. Hydrol. 10 (2), 164–176.

Tromp-van Meerveld, H.J., McDonnell, J.J., 2006. Threshold relations in subsurface stormflow 2: the fill and spill hypothesis: an explanation for observed threshold behavior in subsurface stormflow. Water Resour. Res. http://dx.doi.org/10.1029/2004WR003800.

Tromp-van Meerveld, H.J., Peters, N.E., McDonnell, J.J., 2007. Effectof bedrock permeability on subsurface stormflow and the water balance of a trenched hillslope at the Panola Mountain Research Watershed, Georgia, USA. Hydrol. Process. 21, 750–769. http://dx.doi.org/10.710.1002/hyp.6265.

van Meerveld, H.J., Seibert, J., Peters, N.E., 2015. Hillslope-riparian-stream connectivity and flow directions at the Panola Mountain Research Watershed. Hydrol. Process. http://dx.doi.org/10.1002/hyp.10508.

Van Tassel, J.V., Grant, W.H., 1980. Granite disintegratino, Panola Mountain. Georgia. J. Geol. 88, 360–364.

Waldbauer, J., Chamberlain, P.C., 2005. Influence of uplift, weathering, and base cation supply on past and future CO2 levels. In: Baldwin, I.T., Caldwell, M.M., Heldmaier, G., Jackson, R., Lange, O.L., Mooney, H.A., Schulze, E.D., Sommer, U., Ehleringer, J., Denise Dearing, M., Cerling, T. (Eds.), A History of Atmospheric CO2 and Its Effects on Plants, Animals, and Ecosystems. Ecological Studies, Springer New York, pp. 166–184.

Welch, L.A., Allen, D.M., 2014. Hydraulic conductivity characteristics in mountains and implications for conceptualizing bedrock groundwater flow. Hydrogeol. J. 22, 1003–1026. http://dx.doi.org/10.1010.1007/s10040-10014-11121-10045.

West, N., Kirby, E., Bierman, P.R., Slingerland, R., Ma, L., Rood, D., Brantley, S.L., 2013. Regolith production and transport at the Susquehanna Shale Hills Critical Zone Observatory: part 2 - insights from meteoric 10Be. J. Geophys. Res. Earth Surf. 118, 1–20.

West, N., Kirby, E., Bierman, P.R., Clarke, B.A., 2014. Aspect-dependent variations in regolith creep revealed by meteoric ^{10}Be. Geology 42 (6) http://dx.doi.org/10.1130/G35357.G35357.35351.

White, A.F., 2008. Quantitative approaches to characterizing natural chemical weathering rates. In: Brantley, S.L., Kubicki, J.D., White, A.F. (Eds.), Kinetics of Water-rock Interaction. Springer, New York, pp. 469–544.

White, A.F., Blum, A.E., Schulz, M.S., Vivit, D.V., Stonestrom, D.A., Larsen, M., Murphy, S.F., Eberl, D., 1998. Chemical weathering in a tropical watershed, Luquillo Mountains, Puerto Rico: I. Long-term versus short-term weathering fluxes. Geochim. Cosmochim. Acta 62 (2), 209–226.

White, A.F., Bullen, T.D., Schultz, M.S., Blum, A.E., Huntington, T.G., Peters, N.E., 2001. Differential rates of feldspar weathering in granitic regoliths. Geochim. Cosmochim. Acta 65, 847–869.

White, A.F., Blum, A.E., Schulz, M.S., Huntingdon, T.G., Peters, N.E., Stonestrom, D.A., 2002. Chemical weathering of the Panola granite: solute and regolith elemental fluxes and the dissolution rate of biotite. In: Hellmann, R., Wood, S.A. (Eds.), Water-rock Interaction, Ore Deposits, and Environmental Geochemisty: A Tribute to David A. Crerar. Geochemical Society, St. Louis, MO.

Yesavage, T., Stinchcomb, G.E., Fantle, M.S., SAk, P.B., Kasznel, A., Brantley, S.L., 2016. Investigation of a diabase-derived regolith profile from Pennsylvania: mineralogy, chemistry and Fe isotope fractionation. Geoderma 273, 83–97. http://dx.doi.org/10.1016/j.geoderma.2016.03.004.

Yoo, K., Mudd, S.M., 2008. Toward process-based modeling of geochemical soil formation across diverse landforms: a new mathematical framework. Geoderma 146, 248–260.